Hydrophobicity of Rare-earth Oxide Ceramics and their Application in Promoting Sustained Dropwise Condensation and Corrosion and Fouling Mitigation in Hydropower Systems

by

Sami Khan

B.A.Sc. Chemical Engineering
University of Toronto, 2012
S.M. Candidate, Massachusetts Institute of Technology

December 22, 2015

Abstract

Hydrophobic surfaces that are robust can have widespread applications in various industries including energy, hydropower, and transportation. In particular, hydrophobic materials promote dropwise condensation, which results in heat transfer coefficients that can be an order of magnitude higher than those seen in conventional filmwise condensation. Existing durable materials such as metals and ceramics are generally hydrophilic and require polymeric modifiers to render them hydrophobic, but these modifiers deteriorate in harsh environments. Therefore, robust hydrophobic surfaces have been difficult to realize and their widespread applicability has been limited.

In this project, the class of ceramics comprising the lanthanide series rare-earth oxides (REOs) is studied for their hydrophobic potential. The unique electronic structure of the rare-earth metal atom inhibits hydrogen bonding with interfacial water molecules resulting in a hydrophobic hydration structure where the surface oxygen atoms are the only hydrogen bonding sites. Despite being inherently hydrophobic, the presence of excess surface oxygen on REOs can lead to increased hydrogen bonding and thereby reduce their hydrophobicity. Using X-ray Photoelectron Spectroscopy (XPS) and wetting measurements, surface stoichiometry and surface relaxations have been shown to impact wetting properties of REOs. Specifically, freshly sputtered ceria is shown to be hydrophilic due to excess surface oxygen (shown to have an O/Ce ratio of ~3), which when relaxed in a clean, ultra-high vacuum environment isolated from airborne contaminants reaches close to stoichiometric O/Ce ratio (~2.2) and becomes hydrophobic. Further, airborne hydrocarbon contaminants do not exclusively impact the wetting properties of REOs, and relaxed REOs are intrinsically hydrophobic.

This project also demonstrates that thin-film coatings (~300 nm) of relaxed hydrophobic REOs show sustained dropwise condensation behavior for over 100 hours at accelerated saturated steam conditions without compromising structural integrity or hydrophobicity, and produce an almost tenfold enhancement in the heat transfer co-efficient (103 ± 5 kW/m^2K) compared to conventional filmwise condensation (usually <10 kW/m^2K). It is envisioned that robust hydrophobic rare-earth oxide ceramics will have far reaching technological applications, especially in dropwise condensation and fouling mitigation in hydropower systems.

Acknowledgement:
The information, data, or work presented herein was funded in part by the Office of Energy Efficiency and Renewable Energy (EERE), U.S. Department of Energy, under Award Number DE-EE0002668 and the Hydro Research Foundation.

The author would also like to acknowledge his steering group mentor Patrick March and his industrial mentor Allen Skaja for valuable advice and input throughout the project. The author also acknowledges Deborah Linke and Brenna Vaughan for their support.

Table of Contents

List of Figures

List of Tables

List of Abbreviations

CA – Contact Angle
CAH – Contact Angle Hysteresis
CTE – Coefficient of Thermal Expansion
REE – Rare-earth Elements
REO – Rare-earth Oxides
XPS – X-ray Photoelectron Spectroscopy
SEM – Scanning Electron Microscopy

1. Introduction

Interfaces are ubiquitous -- from industrial surfaces such as turbine blades to household surfaces such as non-stick cookware. Defined as the boundary between two phases of matter, two-dimensional interfaces possess unique physicochemical properties that differentiate them from the otherwise three-dimensional bulk matter. Fundamental interactions at the interface gives rise to the broader "interfacial phenomena" that is two-dimensional in nature. Catalysis, drugs, colloids, foams are all illustrations of interfacial phenomena and have been widely studied under the branch of interfacial science.

One such interfacial phenomenon is the interaction of liquids with solid phases. Broadly speaking, the interaction between water and solids in particular can be classified as *hydrophilic* or *hydrophobic*. The words *hydrophilic* and *hydrophobic,* derived from Ancient Greek, literally mean *water-loving* and *water-fearing* respectively. Materials which have affinity for water are known as *hydrophilic* materials, and cause water to spread across them, maximizing contact. Most materials tend to be hydrophilic -- metals, for example, usually spread water upon contact. Those that tend to repel water and cause water to bead up are known as *hydrophobic* materials. A common example of a hydrophobic material in nature is the lotus leaf: with a slippery, waxy coating on the surface it is capable of keeping itself remarkably dry. Another example is the wing of the Morpho butterfly (*Morpho didius)* (see Figure 1-1)[1]. A more common household example is the protective wax layer often applied on cars. In fact, mechanics often recommend splashing the surface of the car with water to identify if it needs waxing -- if water spreads then it likely needs to be waxed, but if it forms beads of water it is hydrophobic and does not need waxing.

Figure 1-1: Water drop impacting a hydrophobic butterfly wing[1]

For decades, hydrophilic and hydrophobic materials have been extensively studied for applications in a wide range of settings. Both classes of materials can have a significant impact on the performance of power plants, hydropower systems, airplane wings and desalination plants, among other technologies. Improvements in hydrophilic and hydrophobic surfaces could provide better containers with liquids gliding out easily, anti-fog goggles, weather-resistant fabrics, corrosion and fouling resistant surfaces in hydropower systems, or power plants that harness lesser fuel to generate more electricity.

In this project, a particular class of hydrophobic ceramics called *rare-earth oxides* has been studied for aspects of their surface chemistry as well as broader applications.

1.1 Motivation

Hydrophobic materials typically possess low surface energy and have an eclectic range of applications as discussed earlier. Superhydrophobic surfaces in particular, which require a combination of surface chemistry and surface topography, have attracted

significant attention over the past decade because of their broad technological potential[2–6]. There has been considerable focus on understanding their wettability[7,8] and developing them for a wide range of applications including droplet impact resistance, [9–11,1,12,13], anti-icing[14–19], drop-wise condensation[20–24], electro-wetting[25,26], drag reduction[27–32], evaporation [33,34] and anti-corrosion[35–38].

1.1.1 Condensation Heat Transfer and Power Generation

Fossil fuels such as coal, natural gas and oil, under the umbrella term "conventional energy sources", have for decades addressed electricity generation needs: presently accounting for about 67% of the needs in the US and about 87% worldwide [39,40]. Owing to their limited supply and the ever-increasing greenhouse gas emissions, policymakers have been forced to re-evaluate the use of fossil fuels and consider alternative forms of energy such as solar, geothermal and wind energy. While modern research in conjunction with new incentive programs continue to bring alternative forms of energy to fruition, the basic conundrum remains: is the proposed renewable energy mix sufficient to completely end reliance on fossil fuels in the near future? Some studies have estimated it will take several decades to make this transition: the world's energy reliance on fossil fuels barely changed from 88% to 87% between 1990 and 2012[40]. This is a staggering reality, which suggests that conventional energy is here to stay at least in the near future and as such, any efficiency enhancements in conventional electricity generation are highly desirable.

For years, researchers have studied ways to improve energy efficiency in conventional power plants in order to maximize the energy generation output for a given fuel input. Succinctly put, in a conventional power plant, the heat of combustion from

fossil fuels is utilized to boil water and convert to high-pressure steam, which then drives turbines to generate electricity. The steam then condenses to water, which is recycled back to the boiler (See Figure 1-2).

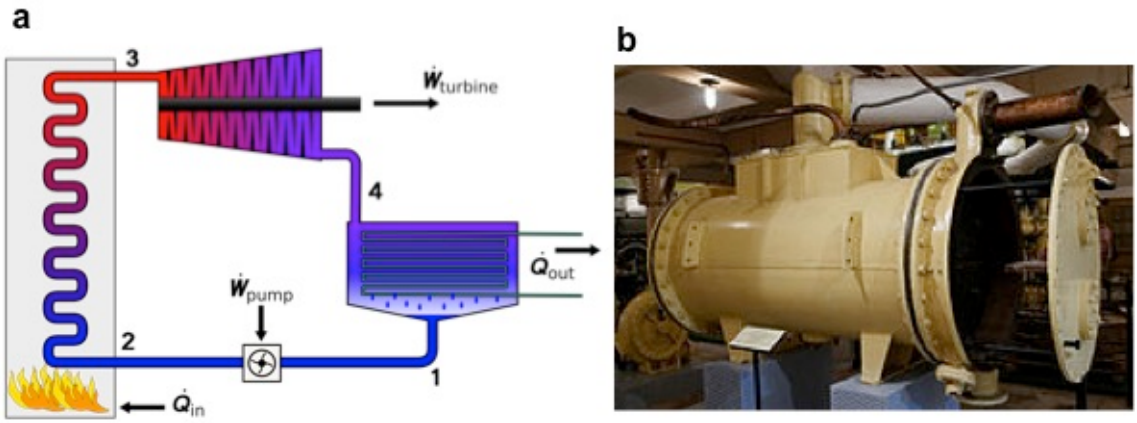

Figure 1-2: Condensation heat transfer in power plants a) Typical Rankine cycle in power plants showing the main steps: 1-2: pumping water from low to high pressure, 2-3: boiling, 3-4: steam running the turbine, 4-1: condensation of steam and b) typical condenser used in power plants

This condensation process is crucial in the overall power plant infrastructure, as roughly 85% of the global installed base of electricity generation plants rely on steam condensers to generate a low backpressure at the outlet of a steam turbine[41]. Traditionally, steam condensers have been constructed from high surface-energy metals such as copper and titanium, which are typically hydrophilic. As such, steam condenses in a film-wise manner on these metals (see right side of Figure 1-3). The presence of this hydrophilic film is very detrimental to process efficiency: using the analogy of an uncomfortable jacket on a hot summer day, this film adds significant resistance to heat transfer and prevents steam from condensing on the underlying surface, thereby reducing heat transfer performance.

If steam were instead made to condense on a hydrophobic material, it would do so in a "drop-wise" manner – as seen below on the left side of Figure 1-3. These drops shed very quickly and expose more of the underlying surface to steam, thereby significantly reducing thermal resistance and improving heat transfer performance. Hydrophobic materials coated over existing condenser surfaces can increase the corresponding heat transfer co-efficient by ten times[42], which in turn corresponds to a superior improvement in the overall plant efficiency by a remarkable 3-5%.

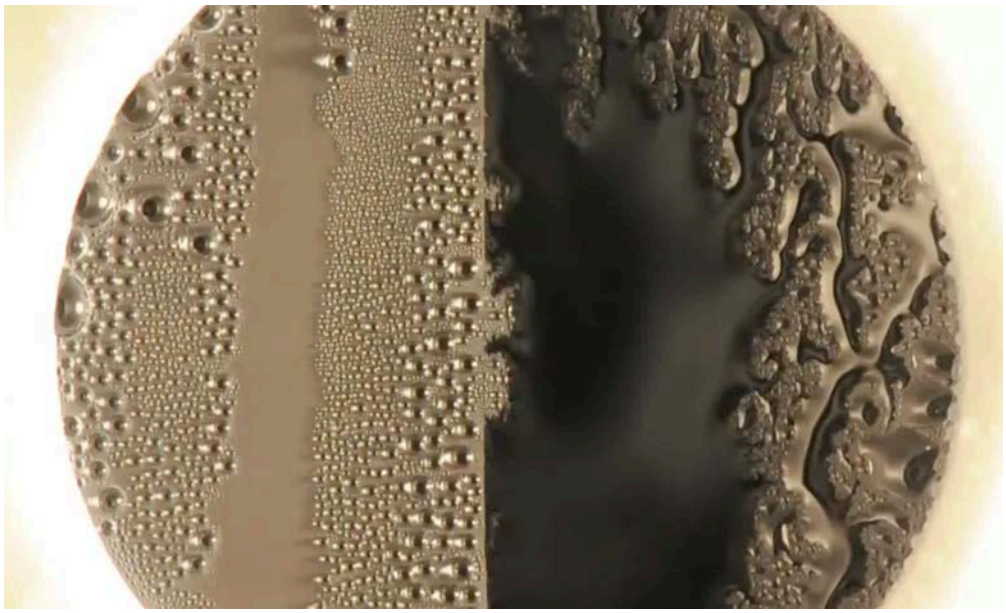

Figure 1-3: Dropwise vs. filmwise condensation. A silicon wafer with one half is covered in a thin layer of fluorosilane (a hydrophobic material) on the left, and the other half cleaned with oxygen plasma on the right (hydrophilic)[43]

1.1.2 Hydropower Industry – Corrosion and Fouling Mitigation

Hydropower has provided a clean, alternative form of energy for many years that still continues to meet the ever-increasing global electricity demand. Presently, hydropower accounts for about 7% of the electricity needs in the U.S, and is a vital component of the clean-energy mix; representing about 52% of the total renewable

energy generation[44]. Hydropower turbines have over the years evolved to become extremely efficient. With over 90% net efficiency, hydropower systems have served as an excellent model for harnessing maximum potential while maintaining a high standard of performance and reliability.

Despite these high performance metrics, hydropower systems have not been immune from environmental factors that affect long-term performance and increase annual maintenance costs. A common example is bio-fouling -- in particular, infestation by zebra mussels in many North American hydropower facilities[45]. These species rapidly adhere to hydropower conveyance structures such as penstocks as well as inside cooling water systems for turbines (see Figure 1-4 below). Some plants have adopted chemical treatment procedures to mitigate the infestation; however, such methods have large annual operating costs (estimated around US$100,000 per year), and may have detrimental environment effects[45].

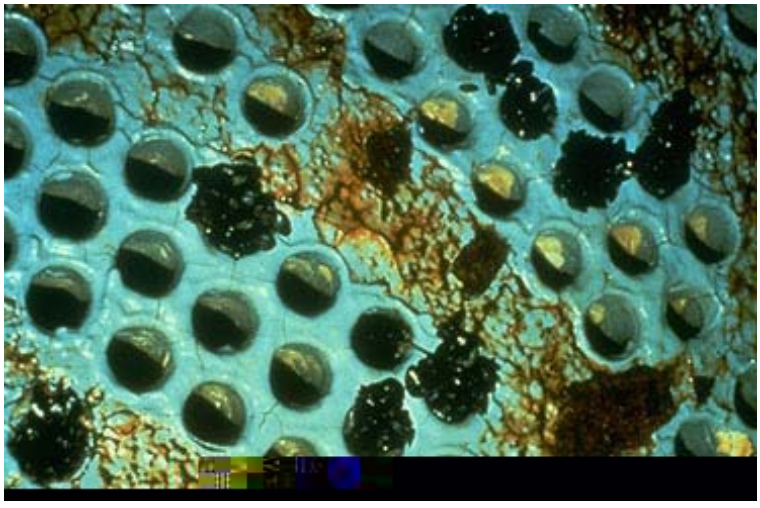

Figure 1-4: Zebra mussel fouling on a condenser tube sheet[45]

Corrosion of plant components, drag-induced losses and scale-formation are other issues that potentially affect the performance of hydropower systems. Several studies

over the past decades have shown that the costs associated with corrosion are high both from an operational and safety perspective. Typical numbers are on the order of 3% for a given country's Gross National Product, and in the United States this amounts to over $276 billion per year[46,47]. Similarly, fouling results in significant operational losses due to impaired heat transfer, flow blockage, and decreased equipment lifetime. Moreover, the costs of heat exchanger fouling arising from cleaning, fluid treatment, additional hardware, and loss of energy and production have been estimated to be about 0.25% of the GDP of industrialized countries[48]. In fact corrosion and fouling are coupled and each exacerbates the effects of the other. Despite the many advances that have been made in corrosion protection, there is still a significant need for the development of robust materials that can overcome the current challenges. A major obstacle for the advance is the lack of understanding of the fundamental interfacial interactions and the ability to dynamically address these interactions.

Thus, it is highly desirable to have a long-term robust solution in the form of infrastructural upgrades and reliable low-surface energy/hydrophobic coatings that can address some of these challenges and thereby reduce net annual costs for the industry and improve performance and efficiency.

1.1.3 The Need for Robust Hydrophobic Materials

An important challenge for broad applicability of hydrophobic materials is their limited robustness[4,5,49]. Most approaches for fabricating superhydrophobic surfaces involve texturing a polymeric hydrophobic material or coating a textured hydrophilic material with a polymeric hydrophobic modifier such as organosilanes or thiols. Existing durable materials such as metals and ceramics are generally hydrophilic and require

polymeric hydrophobic modifiers to render them hydrophobic[50]. However, polymeric modifiers deteriorate in harsh environments such as steam, making it difficult to realize robust hydrophobic surfaces. Hence, there is a clear need for robust materials such as ceramics that are intrinsically hydrophobic.

In hydropower systems in particular, robust material surfaces that can minimize polar interactions (in other words, maximize hydrophobic interactions) can have significant impact on corrosion and fouling mitigation. However, there are many fundamental material science barriers that have to be overcome for the realization of these benefits. For example, low surface energy polymers dominate the field of hydrophobic materials. These polymeric materials lack the stability and durability to last in aggressive environments that include temperature fluctuations, abrasion, erosion, wear, and so on. As discussed previously, these polymeric coatings do not last long in harsh environments; hence robust hydrophobic/superhydrophobic surfaces have been difficult to realize and their widespread applicability has been limited. Therefore, there is a significant need for developing intrinsically hydrophobic or low surface robust materials for controlling fouling and corrosion.

Recent studies have shown that the class of ceramics comprising the lanthanide series rare-earth oxides (REOs) is intrinsically hydrophobic[51–56]. Ceramics have a greater robustness advantage than most polymers when it comes to temperature and abrasion resistance. REO-based cermaics are capable of sustaining their intrinsic hydrophobicity after exposure to extreme processing conditions such as high temperature, abrasive wear, and steam[51].

Little work has been done in the past to better understand the intrinsic hydrophobicity of REOs and the role of surface chemistry changes and environmental factors such as airborne hydrocarbons. Furthermore, no past studies have demonstrated long-term sustained dropwise condensation on REOs and addressed the feasibility of their realistic applications in the industry with a focus on material costs. This leads to the main focus of this project.

1.2 Project Objectives

Succinctly stated, the main objectives of this project are:

- Study the intrinsic hydrophobicity of REOs and demonstrate that airborne hydrocarbons that may accumulate on their surface do not exclusively explain their hydrophobicity
- Study the effect of excess hydrogen-bonding sites such as a higher-than-stoichiometric lattice oxygen content that may affect the wettability of REOs
- Develop stable thin-films of REOs that do not degrade when exposed to harsh environments
- Perform extended steam condensation experiments on hydrophobic REOs to demonstrate dropwise condensation performance and longevity
- Derive inferences for viability of hydrophobic REO coatings in hydropower systems

1.3 Report Layout

In this report, Chapter 1 has introduced the subject of hydrophobic materials and provided a broader motivation for the work, as well as the specific objectives.

Chapter 2 “Review of Wetting and Adhesion” discusses some of the fundamental concepts in interfacial science such as contact angle, surface energy, adhesion, superhydrophobicity and so on.

Chapter 3 “Fundamental Studies on the Hydrophobicity of Rare-earth Oxides” begins by surveying previous work that has studied the wettability of REOs. It will then describe experiments that were performed to demonstrate that REOs are intrinsically hydrophobic, and that ambient airborne hydrocarbons do not exclusively explain their hydrophobic behavior. The effect of morphological and surface chemistry defects will be studied as well.

Chapter 4 “Sustained Drop-wise Condensation on REOs” describes experiments that were performed to study condensation behavior and heat transfer performance on hydrophobic REOs.

Finally, Chapter 5 “Summary and Conclusions” will summarize the main take-away points from this project.

2. Review of Wetting and Adhesion

In this chapter, fundamental concepts in wetting and adhesion will be reviewed.

2.1 Fundamentals of Wetting

The phenomenon of wetting has been known for many centuries. Aristotle first reported around 300 BC that when a thin solid object that is denser than water is laid on the surface of water, it will float[57]. Galileo, in 1612, further noted that the top of such a floating solid was typically below the surface of the water[57]. This phenomenon arises due to a unique property of water called "surface tension" -- which provides a force at the contact line surrounding the floating object.

2.1.1 Young's Model

Thomas Young, in 1805, was the first to explicitly quantify wettability in form of an interfacial property called "contact angle".

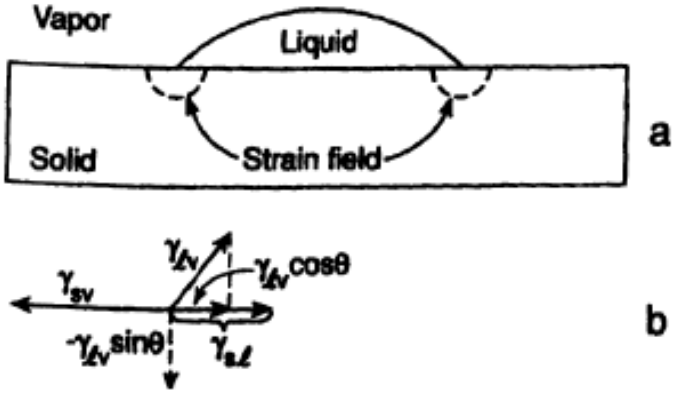

Figure 2-1: Young's wetting model (a) Sessile drop of liquid on a solid, showing the strain field in the solid under the three-phase boundary. (b) Complete resolution of forces about a three-phase line[57]

Essentially, Young's model is a two-dimensional force balance at the contact line of a droplet (Figure 2-1). This force balance relates the three principal interfacial

energies: the liquid-vapor interfacial energy γ_{LV}, the solid-liquid interfacial energy γ_{SL}, and the vapor-solid interfacial energy γ_{SV}. With regards to a vertical force balance, the vertical forces due to γ_{LV} are balanced by the strain field below the contact line, assuming that the solid material is rigid and non-deformable. Therefore, the horizontal force balance results in the famous Young equation:

$$\gamma_{SV} = \gamma_{SL} + \gamma_{LV} \cos \theta_e \qquad \text{Equation 2-1}$$

where, θ_e is known as the equilibrium or static contact angle, and is a property of given solid-liquid pair.

The principles of *hydrophilicity* and *hydrophobicity* introduced earlier can be quantified using θ_e. By convention:

Hydrophilic materials: $0° < \theta_e < 90°$

Hydrophobic materials: $90° < \theta_e < 180°$

It can be further inferred from the Young's equation that θ_e depends on interfacial energies γ, which is the free energy per unit area. In a liquid, each molecule in the bulk is pulled equally in every direction by neighboring liquid molecules, resulting in a net force of zero. However, on the surface, molecules do not have neighbors in all directions to provide a net balanced force and as such, they are pulled inwards by neighboring molecules creating a "tension". As a result, the liquid contracts its surface area to maintain the lowest possible surface free energy. This intermolecular force to contract the surface is called "surface tension" and is responsible for the shape of liquid droplets (see Figure 2-2).

Figure 2-2: Model of intermolecular forces in a liquid drop on a surface. Surface tension is caused by the unbalanced forces of liquid molecules at the surface, which are clearly different than those at the bulk[58]

The differences between surface tensions of common liquids provide insight into the nature of intermolecular forces in these liquids. For example, hydrocarbon liquids such as hexane and octane tend to have the lowest surface tensions among all known liquids, usually less than 25 mJ/m^2. On the other hand, water at 25°C has a surface tension of 72 mJ/m^2. The difference can be explained by the nature and strength of intermolecular forces: water tends to have hydrogen-bonding networks among its molecules due to the electronegative character of the oxygen atoms and the electropositive characters of hydrogen atoms in water giving rise to this dynamic interaction (See Figure 2-3). Hydrocarbon liquids do not possess such intermolecular forces of attraction, and as such their surface tension is lower. Liquid mercury has an even higher surface tension of 465 mJ/m^2, which can be explained by the high strength of metallic bonding in liquid mercury.

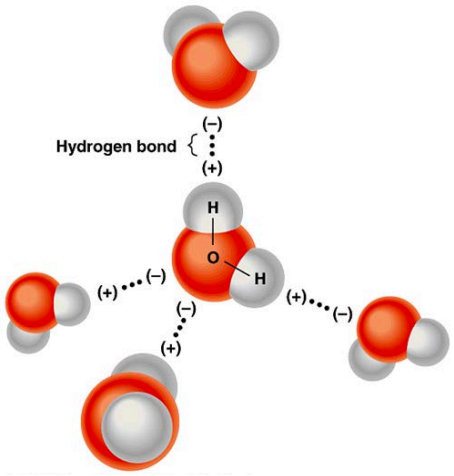

Figure 2-3: Hydrogen bonding interactions between water molecules

For solids, the interfacial energy is more commonly known as "surface free energy". Most solids possess free surface energies that are much larger than water. Metals such as aluminum and copper have surface energies of 1.14 and 1.78 J/m^2 respectively[59]. This explains why water typically spreads on these metals. On the other hand, on materials with a low surface energy such as polytetrafluoroethylene (PTFE, or Teflon®), with free surface energy of about 0.020 J/m^2, water beads up[60]. Typically, hydrophobic materials are known to possess low surface energy, which makes them attractive for repelling both water and solids.

2.1.2 Advancing and Receding Contact Angles and Contact Angle Hysteresis

While Young's equation provides a first-principles understanding of wetting on a theoretical "smooth" surface, in reality most solid surfaces possess significant heterogeneities, either due to chemical imperfections or roughness. Even the most well-polished single-crystal solid surfaces such as a chip of Yttria-stabilized Zirconia (YSZ) possesses heterogeneities and micro and nano-scale roughness. These heterogeneities act as "pinning sites" for the contact line of a drop and when a moving drop encounters these defect sites, it can assume a contact angle that may be higher or lower than the

equilibrium contact angle θ_e postulated by Young's theory. As such, the measurement of a single static contact angle to characterize wetting behavior is not particularly adequate in realistic situations.

Thus, in order to address these drawbacks, a new type of characterization of wettability is needed in terms of "dynamic" contact angles. Specifically, it is important to define the contact angles formed by expanding and contracting liquids, and are referred to as the *advancing contact angle* θ_a and the *receding contact angle* θ_r respectively (See Figure 2-4). The advancing angle θ_a, is simply the maximum observed contact angle attained by a drop, whereas the receding angle is the minimum observed contact angle attained. The difference between the advancing angle and the receding angle is called contact angle hysteresis (CAH) = $\theta_a - \theta_r$. The significance of CAH is that it represents the degree of drop pinning sites on the surface and governs the ease at which a drop can roll off a surface. For solids that have a low CAH, water drops shed relatively easily from the surface given that pinning sites are minimal.

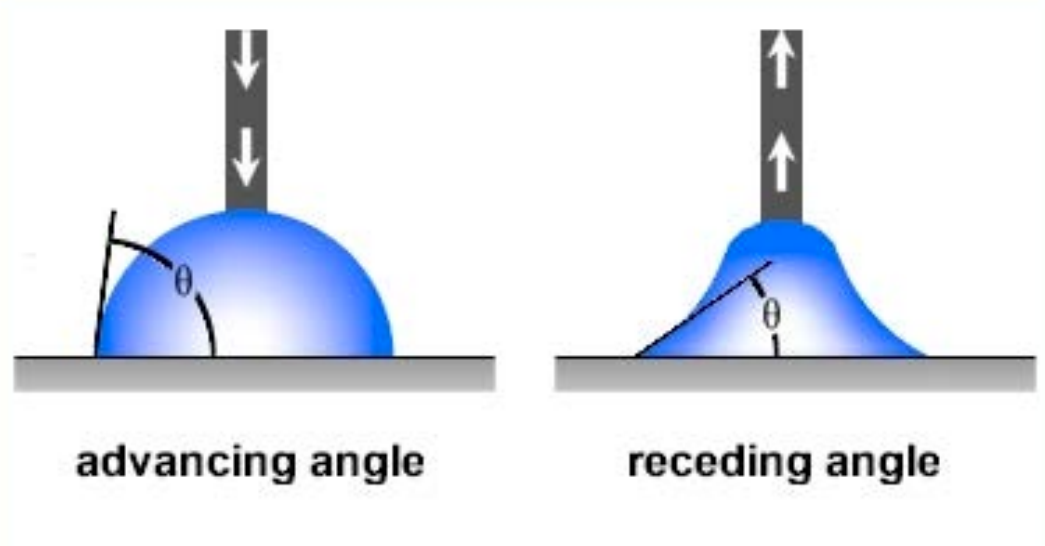

Figure 2-4: Illustration of advancing and receding contact angles

It is well known that the experimentally measured advancing contact angle θ_a is a good approximation of Young's theoretical equilibrium contact angle θ_e and as such a better measure of hydrophobicity versus hydrophilicity[58,61,62]. In this project, all experimentally measured contact angle values are the advancing contact angles and have been used to characterize wettability.

2.1.3 Wenzel and Cassie Models for Rough Surfaces and Superhydrophobicity

Surface heterogeneities also exist in terms of roughness, which complicates Young's contact angle model further. The apparent contact angle of a droplet on a surface relies greatly on the wetting state of the droplet and the morphology of the surface. The two most common models of wetting states that incorporate the effect of roughness are the "Wenzel" and "Cassie-Baxter" models.

In the Wenzel state (Figure 2-5), the roughness features on the surface impale the drop within the features. As such, the drop may demonstrate a high contact angle, albeit it will be highly pinned on the surface. The change in contact angle owing to the Wenzel state is given by the following equation:

$$\cos \theta^* = r (\cos \theta_e) \qquad \text{Equation 2-2}$$

Where

r = "Roughness factor" = Total surface area/Projected surface area (always ≥ 1)

θ^* = Apparent contact angle due to roughness effects in Wenzel state

θ_e = Theoretical equilibrium contact angle

It can be seen that in the limiting case where $r = 1$, the surface is perfectly smooth and the apparent contact angle is equal to the Young's equilibrium angle. This relation also implies that any roughness will *amplify* a solid's intrinsic wettability. In other words,

a hydrophilic solid ($\theta_e < 90°$) will become even more hydrophilic ($\theta^* < \theta_e$) whereas a hydrophobic solid ($\theta_e > 90°$) will become even more hydrophobic ($\theta^* > \theta_e$).

The other commonly used model – the Cassie-Baxter model – postulates that the drop sits *on top* of the roughness features rather than sinking inside (see Figure 2-5). As such, there is a composite of liquid/vapor and liquid/solid interfaces and the drop is not quite pinned as compared to the Wenzel state. The change in contact angle owing to the Cassie-Baxter state is given by the following equation:

$$\cos \theta^* = \varphi(1 + \cos \theta_e) - 1 \qquad \text{Equation 2-3}$$

Where,

φ = wetted area fraction

θ^* = Apparent contact angle due to roughness effects in Wenzel state

θ_e = Theoretical equilibrium contact angle

Similar to the Wenzel state, the Cassie-Baxter state amplifies the intrinsic wettability of solids. In fact, if solids exhibit the Cassie-Baxter state in the hydrophobic regime with $\theta^* > 150°$, they are often referred to as *superhydrophobic* materials. Many surfaces in nature such as the lotus leaf and wings of the Morpho butterfly as discussed earlier possess roughness features and intrinsic hydrophobicity, and as such demonstrate superior water-repellency with $\theta^* > 150°$. This extremely high apparent contact angle is accompanied by very low contact angle hysteresis. As such, superhydrophobic materials especially those that mimic such surfaces found in nature, are highly attractive for research and industrial applications.

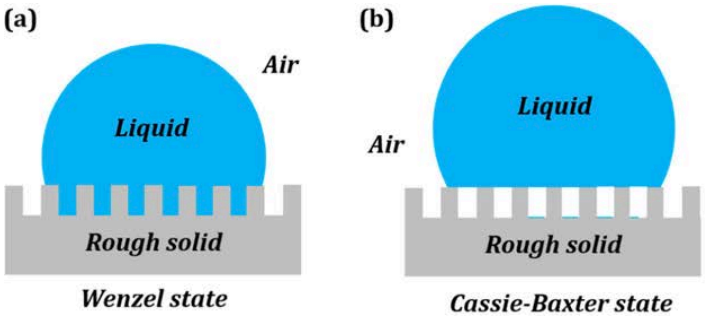

Figure 2-5: Commonly used models for rough surfaces (a) Wenzel state model where the water drop impales within the roughness features and (b) Cassie state model where the water drop sits atop roughness features

In this project, all contact angles were measured using an instrument called the *goniometer* (Rame-Hart M500 series - See Figure 2-6). Water drops dispensed on the solid surface of interest are illuminated using a lamp and recorded by a live camera. An in-built software recognizes the drop and surface and measures the contact angle. Both advancing and receding contact angles can be measured by dispensing liquid to or withdrawing fluid from the drop respectively.

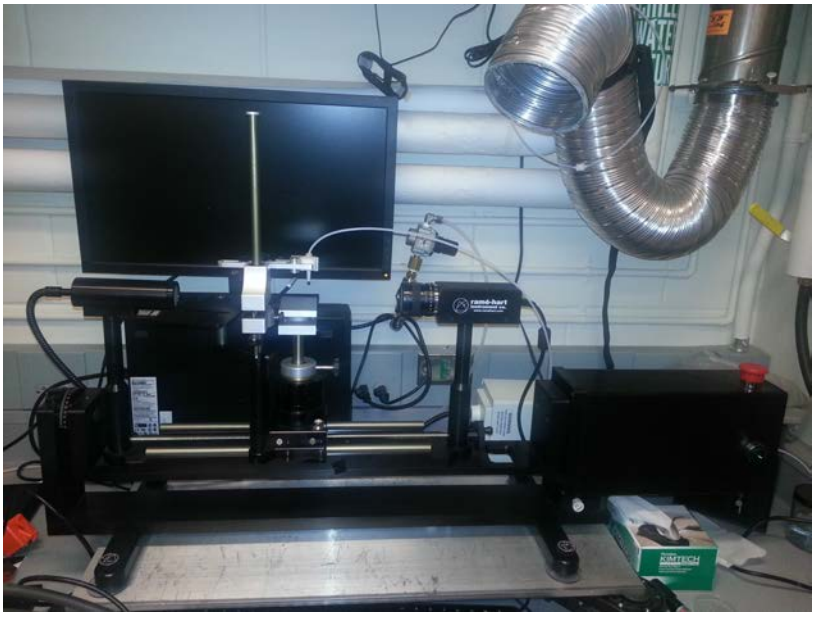

Figure 2-6: Goniometer used to measure contact angles

2.1.4 Adhesion

Intuitively, low-surface energy hydrophobic materials are attractive in repelling solids as well. Several studies have shown the relation between wettability and solid adhesion. For example, researchers found that the ice adhesion strength (force required to fracture ice from a surface) scales with the cosine of the receding contact angle[14] as seen in Figure 2-7. Another study found a positive correlation between marine biofouling fracture energy and contact angle hysteresis[63].

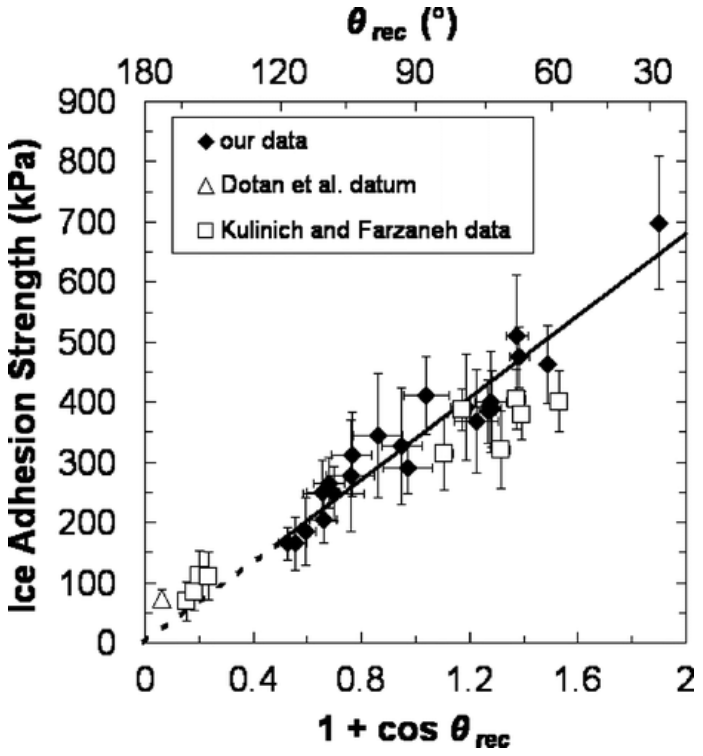

Figure 2-7: Correlation between Ice Adhesion Strength and Water Wettability[14]

It is therefore hypothesized that low-surface energy hydrophobic materials also offer promise in repelling solids and as such this makes them attractive for hydropower applications where scale and bio-fouling resistance is important.

3. Fundamental Studies on Hydrophobicity of Rare-earth Oxides (REOs)

In this chapter, fundamental studies on the wettability of rare-earth oxides (REOs) will be detailed. Experiments investigating effect of surface chemistry and ambient airborne hydrocarbons on the wettability of REOs will be discussed. The basic hypothesis of whether REOs are intrinsically hydrophobic will be addressed. Henceforth, rare-earth oxides will be abbreviated as REOs for simplicity.

3.1 What are the rare-earths elements?

Rare-earth elements (REEs) range from lanthanum to lutetium (including scandium and yttrium), and are often called "lanthanide series elements" (see Figure 3-1 below). The adjective "rare" is a misnomer; rare-earth elements are in-fact highly abundant in the earth's crust and are naturally-occurring (with the exception of Promethium which is synthetically made).

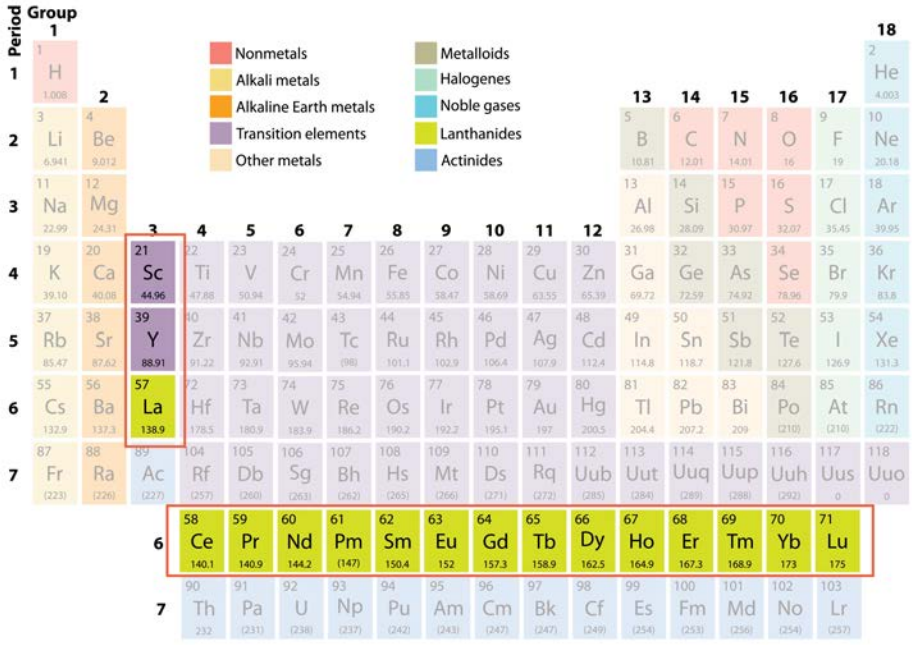

Figure 3-1: The Rare Earth Elements in the Periodic Table

The Japanese have called them "the seeds of technology". The U.S. Department of Energy have called them "technology metals". Senior geologists have gone so far to say they are the "vitamins of chemistry". Unbeknownst to many, REEs have truly evolved as the pillars supporting many of the technological advances today -- from the down-scaling of electronics to the enabling of green energy and medical technologies, and supporting a variety of essential telecommunications and defense systems. Owing to their unique magnetic, phosphorescent, and catalytic properties, REEs have been integral ingredients in enabling many modern technologies to fruition. Some of the most significant applications of REEs include[64]:

- Permanent neodymium magnets which are some of the strongest known magnets and are critical for operation on modern wind turbines and are also used in consumer products such as headphones, hard drives and electric vehicles
- Color monitors for computers, consumer electronics and televisions are dependent on REE phosphors for the colors red (europium), blue (europium) and green (terbium).
- Light emitting diodes (LEDs) that find applications in many electronics use yttrium, terbium and erbium
- Catalysts – REEs in used in many industrial applications: specifically – fluid-cracking catalysts used in the refining of crude oil.

Figure 3-2 shows many more novel areas of applications of REEs[65].

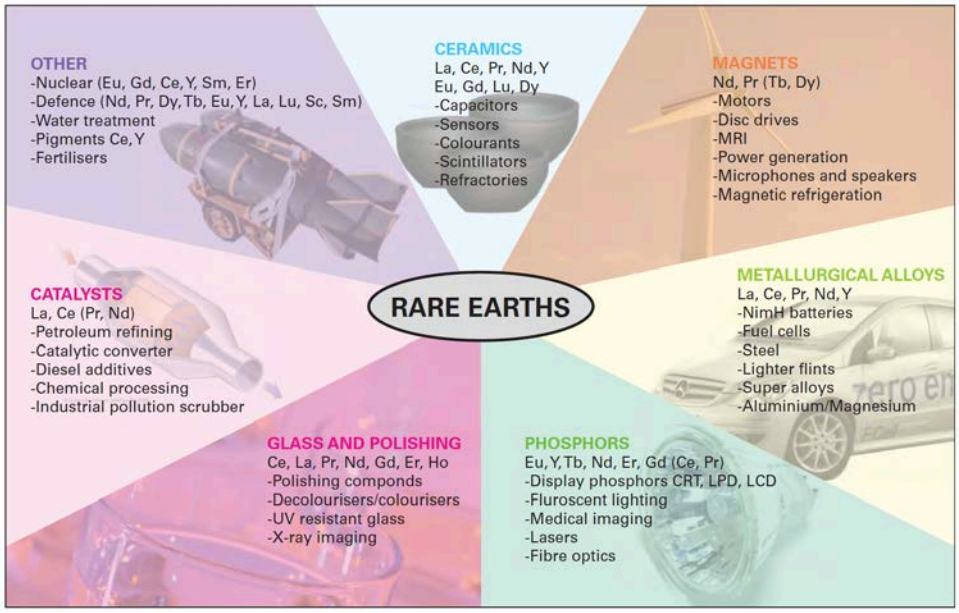

Figure 3-2: Some additional applications of rare-earth elements[65]

3.2 Previous Studies on Hydrophobicity of Rare-earth Oxides

Previous studies have shown that the class of ceramics comprising the oxides of the rare-earth group of elements in the lanthanide series (rare-earth oxides or REOs) is intrinsically hydrophobic[51–56]. An important property that governs a material's surface energy is its polarity: increasing polarity generally leads to increased surface energy and hydrophilicity. Common ceramics and metals tend to have high surface energy and are hydrophilic, as their surfaces are known to have a large number of polar sites due to coordinative unsaturation effects[66–68]. While most common ceramics tend to have high surface energy and are hydrophilic, the unique electronic structure of REOs can minimize polar interactions, inhibit hydrogen bonding with the surface, and render them intrinsically hydrophobic. Other recent studies have found a one-to-one correspondence between surface polarity, and hydrophobicity or hydrophilicity of the surface [69,70].

What makes REOs so different from other metal oxides in terms of their wettability? Metal atoms in REOs have a unique electronic structure: the unfilled 4*f* orbitals are shielded from interactions with the surrounding environment by the full octet of electrons in the $5s^2p^6$ outer shell (See Figure 3-3). This shielding effect minimizes the hydrogen bonding with interfacial water molecules and renders REOs hydrophobic[51] as shown in Figure 3-3. In contrast, in the case of a common ceramic like alumina, the lack of such a shielding effect allows the metal atom to hydrogen bond with interfacial water molecules[69,71]. In this case, water molecules are able to maintain their hydrogen-bonding network on alumina, resulting in hydrophilicity.

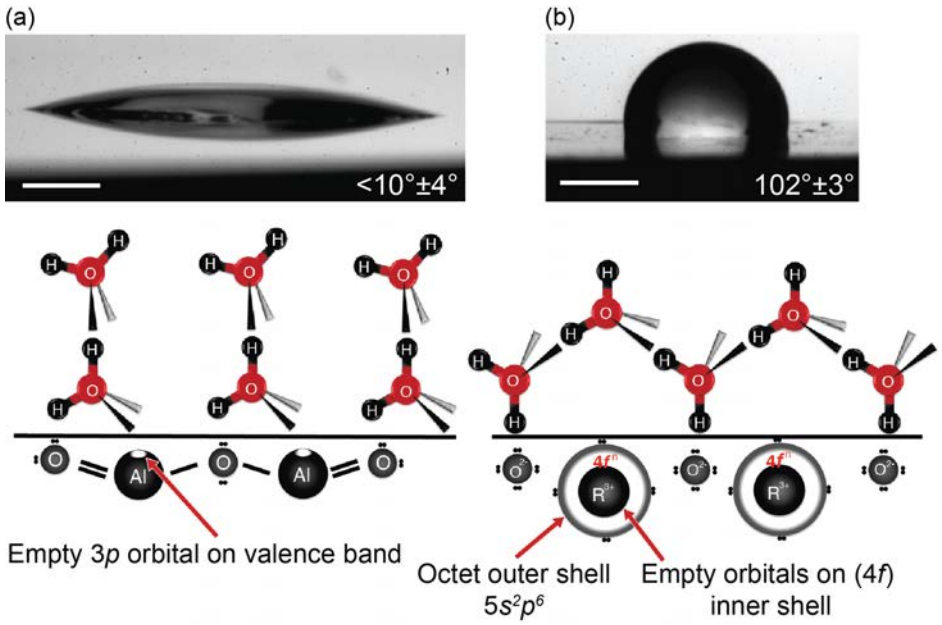

Figure 3-3: Schematic of the orientation of water molecules and the associated wetting properties of a surface (a) Hydrophilicity and schematic of the orientation of water molecules next to an alumina surface (using different scales for the surface and water molecules). (b) Hydrophobicity and schematic of the orientation of water molecules next to neodymia (an REO) (surface and water molecules not to scale)[51]. Scale bars, 1 mm.

Hence, in the case of REOs, water molecules next to the surface cannot maintain their hydrogen-bonding network and attain an *anti-clathrate* hydrophobic hydration structure (Figure 3-3) and in fact, the entire REO series ranging from ceria to lutecia is intrinsically hydrophobic as seen by the macroscopic contact angle (Figure 3-4 (c). The *anti-clathrate* hydration structure has been verified through FTIR/GATR (Fourier transform infrared/grazing-angle attenuated total reflection) measurements[72]. Note that lanthanum is not an *f*-block rare-earth element, and as such lanthanum oxide does not demonstrate hydrophobicity and has not been included in any studied on the wettability of REOs.

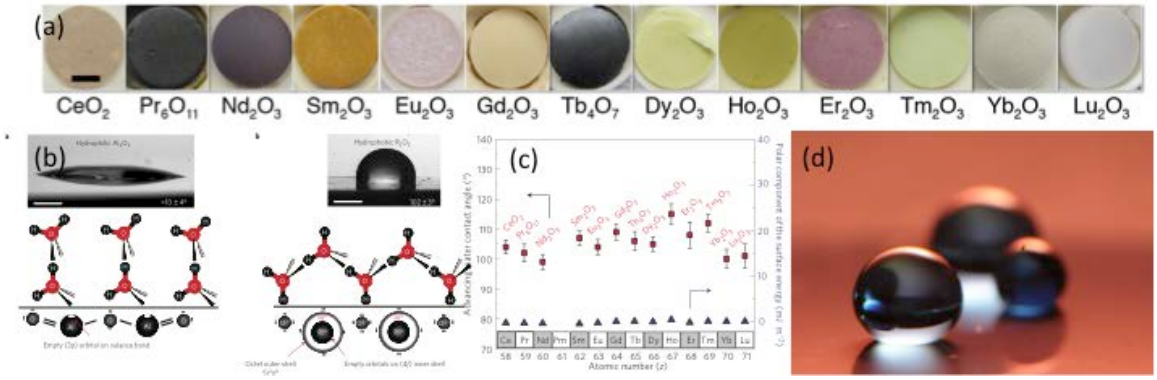

Figure 3-4: Hydrophobicity of the entire rare-earth oxides series from ceria to lutecia (a) photographs of sintered REO pellets synthesized using solid-state chemistry techniques (b) Hydration structure of interfacial water molecules next to a typical ceramic like alumina and rare-earth oxide (c) Surface energy and contact angle data on REOs (d) superhydrophobic REO by conformally coating onto a multiscale-textured surface[72]

In fact, REOs also demonstrate superhydrophobicity when conformally coated on textured surfaces (Figure 3-5) and completely repel high-speed impinging droplets[72]. Superhydrophobic laser-ablated REOs have also been developed[55]. REOs are capable of sustaining their intrinsic hydrophobicity after exposure to extreme processing conditions

such as high temperature, abrasive wear, and steam[72]. Because of the unique electronic properties of the metal atoms in REOs, absence of polar interactions, and their hydrophobic properties, it is hypothesized that REO ceramic based systems can be effective for inhibiting electrochemical reactions and as such are also a unique system to systematically study the impact of electronic structure, defects, and doping on fouling and corrosion and other low-surface energy applications.

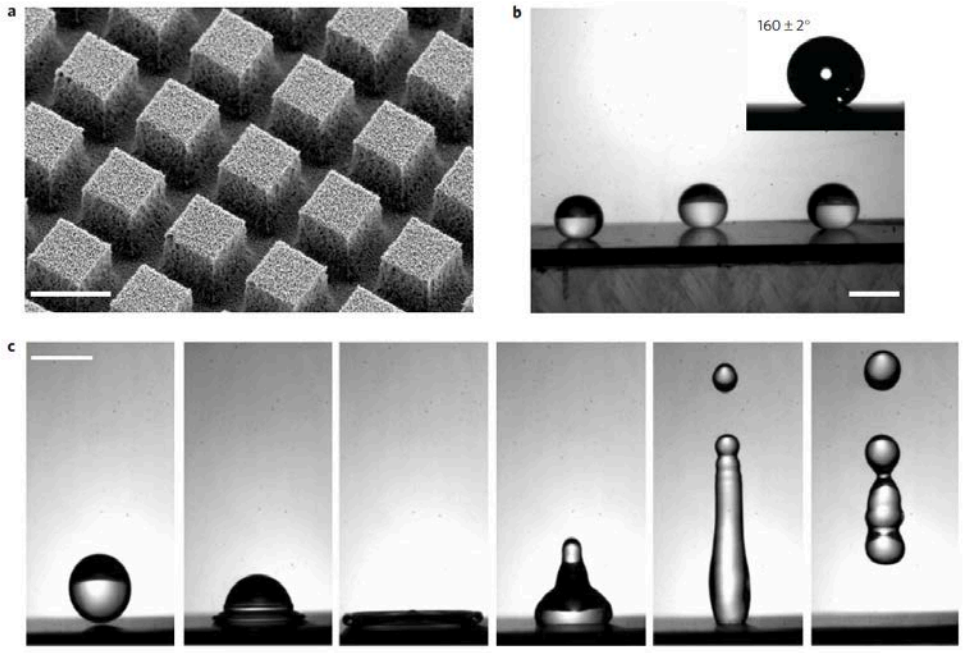

Figure 3-5: (a) Scanning electronic micrograph of a textured surface coated with a thin layer of cerium oxide (~200 nm); scale bar, 10 μm. (b) Photographs of water droplets on the rare-earth oxide surface in (a) (contact angle: ~160°); scale bar, 2.5 mm. (c) Sequential photographs of water droplet impinging at ~1.6 m/s on the surface in (a); Scale bar, 2.5mm.[72]

While previous studies have demonstrated proof-of-principle of hydrophobicity of REOs, little work has been performed on investigating the effect of surface chemistry changes and other environmental factors such as ambient airborne hydrocarbons on their wettability. In light of these previous results, it is worthwhile exploring facets of REO

surface chemistry in relation to their wettability, which has been the focus of the many experiments conducted during this research.

3.3 Thin-Film Fabrication of REOs

In previous studies on REOs, wettability was studied on pellets that were pressed into shape using REO powders[55,72] (see Figure 3-4 (a) for examples of pellets that were fabricated). While pellets are a convenient method of providing an experimental surface to study for wettability using readily available powders, they have a few inherent drawbacks. Firstly, pellet surfaces are composed of numerous grains (see Figure 3-6) and as such they possess both physical and chemical heterogeneities. As discussed previously in Chapter 2, the presence of such heterogeneities affects contact angle measurements. For example, grain boundaries may provide pinning sites for droplets and as such, receding angle measurements are unpredictable and unreliable on pellets. In fact, on a ceria pellet (Figure 3-6 (a)), the measured contact angle hysteresis is 48°, whereas a sputter-deposited thin-film of ceria has a significantly lower hysteresis at 19° given the relative homogeneity and lack of pinning sites as seen in Figure 3-6 (b).

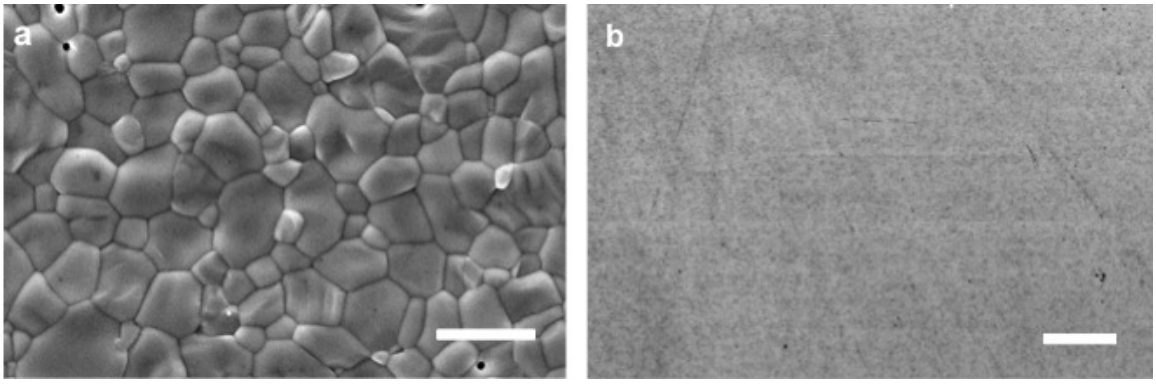

Figure 3-6: SEM comparison of ceria as (a) pellet showing numerous grains (b) sputter-deposited thin-film showing relative homogeneity. Both scale bars are 10 μm

Secondly, pellets are not quite suitable for broader scalable applications. Most industrial surfaces are constructed from robust materials such as metals, and as such any wettability modification on these materials is best realized by means of an overlying coating. This is also more effective from a cost perspective. As such, thin-films of REOs (<1 μm) are more advantageous and throughout this project, thin-films have been fabricated and studied for wettability rather than pellets.

There are many known techniques to deposit thin-films of materials. Commonly used methods include: electron beam deposition, pulsed laser deposition (PLD), atomic layer deposition (ALD), spin coating, and so on. In this project, sputter-deposition has been primarily used as the preferred method to deposit thin films of REOs. Sputter-deposition is best described as playing "billiard balls with ions and atoms" (see Figure 3-7). In this process, a gaseous plasma is first created in a vacuum chamber typically using argon gas. Then, ions from the plasma are accelerated into a bulk solid "target" that is made from the material whose thin-film is being deposited. This material is eroded by the high-energy ions emanating from the plasma via energy transfer and is ejected in the form of particles -- either as atoms, molecules or clusters of both. As these particles are ejected they travel to a "substrate" at the bottom of the sputtering chamber, which is typically a polished silicon wafer.

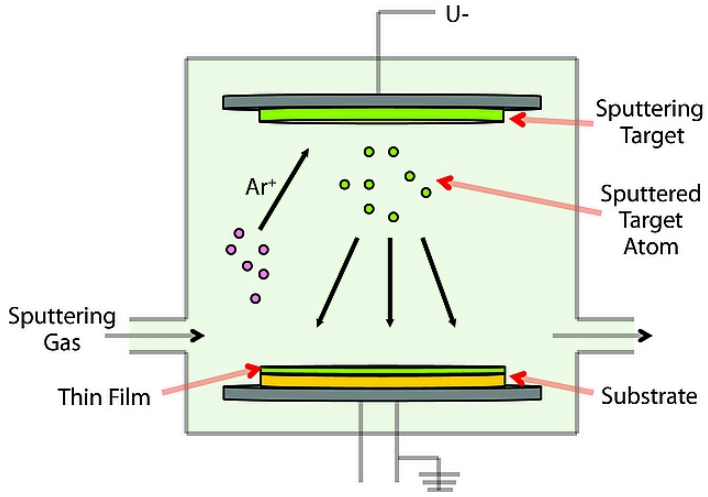

Figure 3-7: Sputter-deposition process in a vacuum chamber

Cerium oxide (also called ceria and henceforth referred to as such) has been chosen as a model REO in this project given the technical feasibility of fabricating thin-films of ceria and considerations of cost and availability of sputtering targets of ceria, as well as the availability of extensive past literature on the surface chemistry of ceria. Erbium oxide (also called erbia) has also been used for thin film-depositions. Typically, thin-films of ~300 nm thickness have been deposited. Figure 3-8 shows a cross-section slice of a ceria thin-film deposited on a silicon wafer as seen in an SEM.

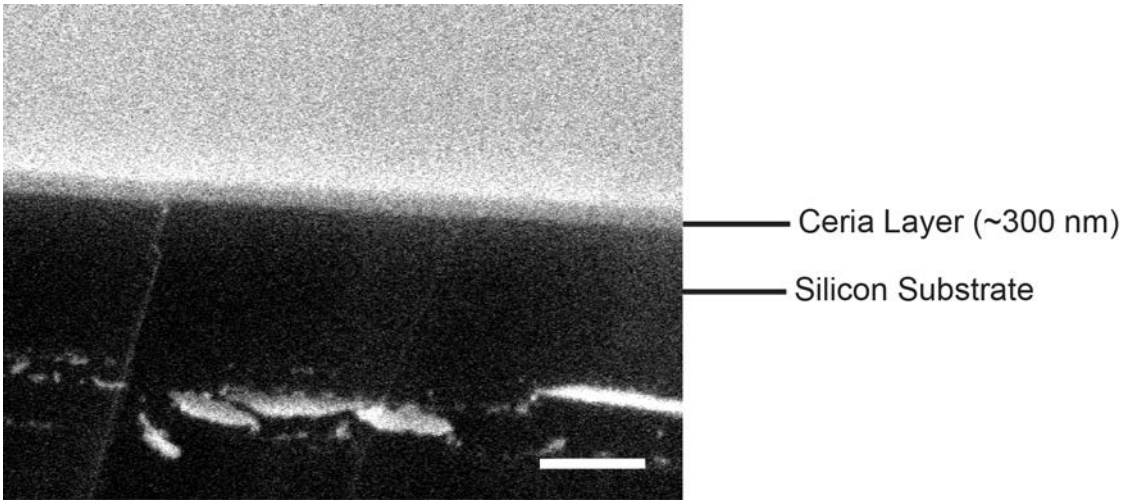

Figure 3-8: SEM cross-section image of a ~300 nm thin-film of ceria on a silicon substrate. Scale bar: 1 μm)

3.4 Surface hydrocarbon content and wettability of REOs

Airborne hydrocarbons in ambient air can originate from both natural and anthropogenic sources such as incomplete combustion. The concentration of these hydrocarbons is typically very dilute compared to the other bulk gases in the atmosphere such as oxygen, and these concentrations range in the parts-per-trillion to parts-per-billion level. Despite their dilute concentrations such hydrocarbons may adsorb on solid surfaces and as such, interfere with wettability. As discussed previously, given that hydrocarbons typically refrain from bonding with water due to their inherent chemical properties, any surface that contains ambient airborne hydrocarbons may show an increase in water contact angle.

As such, there have been concerns in recent literature that the hydrophobicity of REOs may in fact originate from ambient airborne hydrocarbons. Researchers have shown that the contact angle of water measured on REOs increases with time when left in ambient air as it progressively adsorbs atmospheric hydrocarbon contaminants[73]. Therefore, they have attributed the hydrophobicity of REOs to adsorbed hydrocarbon contaminants rather than arising from intrinsic material characteristics of REOs.

While it is important to avoid ruling out the effect of adsorbed surface hydrocarbon contaminants on the wettability of REOs, it is also important to study if hydrocarbon-free REOs indeed demonstrate intrinsic hydrophobicity and characterize their wettability relative to other hydrophilic materials that may also adsorb hydrocarbons. Also, changes in surface chemistry and stoichiometry of a pristine REO surface may potentially impact wettability. As explained previously, hydrophobic materials typically demonstrate unique behaviors such as superhydrophobicity, complete

bounce-off of impinging droplets, dropwise condensation, ice-repellence and so on. If superficial adsorbed hydrocarbons are responsible for these properties then it would be detrimental to realizing viable, long-term applications of hydrophobic REOs. Hence, in order to better understand the contribution of surface hydrocarbon contamination towards the wettability of REOs and demonstrate genuine intrinsic hydrophobicity, the following experiments were carefully designed and conducted.

3.4.1 Comparison between Ceria and Alumina

Surface hydrocarbon levels were compared and contrasted on hydrophobic and hydrophilic materials under identical conditions. Ceria and alumina were selected (which, as described earlier, are intrinsically hydrophobic and hydrophilic, respectively). Approximately 300 nm thick layers of ceria and alumina were sputter-deposited on distinct silicon wafers (AJAsputterer ATC series), and were transported in the same vacuum desiccator for X-Ray Photoelectron Spectroscopy (XPS) analysis in an ultra-high vacuum (UHV) chamber (PHI Versaprobe II XPS). Immediately after XPS measurements, water contact angles (WCA) were measured using a goniometer (Rame-Hart M500 series). As shown in Table 3-1, both surfaces were found to have similar surface carbon content (~15%) measured by XPS, yet only ceria was hydrophobic (WCA > 90°) while alumina was hydrophilic (WCA $\ll$ 90°).

Table 3-1: Effect of surface carbon content: comparison between ceria and alumina

Surface	**Surface atomic carbon content (%)**	**Contact angle (°)**
Ceria	15.1 ± 2.1	104 ± 2
Alumina	15.8 ± 2.5	45 ± 3

These results clearly indicate that surface hydrocarbon contamination exclusively cannot explain the hydrophobicity of REOs. In fact, the ceria sample in this experiment was hydrophobic despite having an almost two-fold lower surface carbon content (~15%) than previously reported values on a hydrophobic ceria surface exposed to ambient air (~34%)[73].

All REO samples used in this project have been controlled and handled carefully to minimize hydrocarbon contamination by storing in vacuum (dessicator chambers at ~100 Pa or less) immediately after they were fabricated, until the point of reasonable experimentation in ambient air. XPS measurements on such samples indicate ~12% carbon on the surface, which is significantly lower than that expected in the case of hydrocarbon contamination-induced hydrophobicity such as steel, as explained further.

3.4.2 Hydrophobicity in pure steam environment and dropwise condensation

Steam is highly aggressive in terms of temperature and pressure and is often use to clean and sanitize surfaces. In fact even silane or thiol based hydrophobic coatings are not robust and degrade in steam environments[24], and as such steam can degrade adsorbed hydrocarbons from the ambient atmosphere. As stated previously, a unique hallmark of hydrophobic materials is sustained dropwise condensation: if a material has adsorbed hydrocarbons that would degrade in the presence of steam, it would not demonstrate dropwise condensation for extended periods of time. Therefore, it can be hypothesized that only genuinely hydrophobic materials whose wettability does not exclusively depend on adsorbed surface hydrocarbons demonstrate sustained dropwise condensation.

In order to test this hypothesis, steel and ceria were compared and contrasted in this experiment. Contact angles were measured on an as-received stainless steel 304

sample and a ceria sputtered silicon wafer and surface hydrocarbon content was measured using XPS. As seen in Table 3-2, the as-received steel sample had a significantly high water contact angle (~85°) due to adsorbed hydrocarbons. In contrast, ceria was hydrophobic (CA > 90°) despite having a lower surface carbon percentage.

Table 3-2: Surface carbon (measured by XPS) and water contact angle

Surface	Surface carbon (%)	Contact angle (°)
Ceria	15.1	101
Steel	50.7	85

Upon steam condensation, ceria showed sustained dropwise condensation while the condensate on the steel sample turned into a film as steam washed away the adsorbed hydrocarbons as shown in Figure 3-6. Furthermore, on the ceria-coated surface, small departing drop sizes and higher condensation heat transfer co-efficients were measured. In fact, as described extensively in Chapter 4, ceria remarkably showed sustained dropwise condensation for over 100 hours without compromising hydrophobicity or structural integrity.

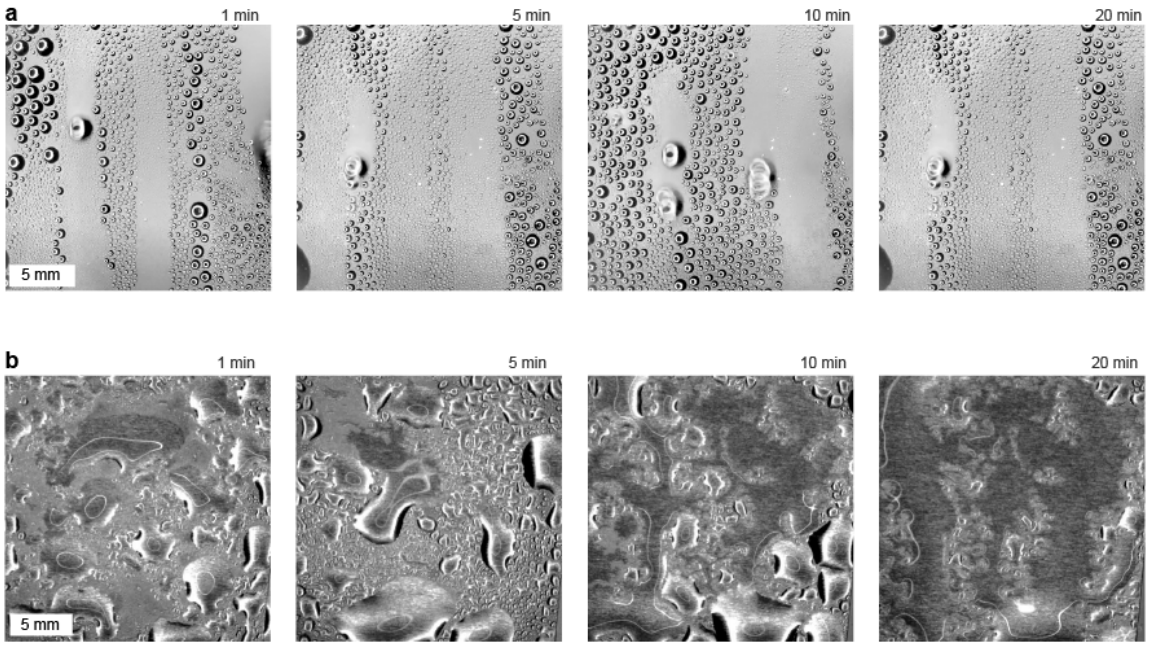

Figure 3-9: (a) sustained dropwise condensation on ceria sputtered silicon wafer (b) adsorbed hydrocarbons washed away by steam on stainless steel sample and the resulting condensation is filmwise.

This experiment demonstrates that while surface hydrocarbons can greatly increase the contact angle of hydrophilic materials such as steel, they are unstable and their degradation in steam results in filmwise condensation. On the contrary, there is an element of intrinsic hydrophobicity in REOs that shows sustained dropwise condensation.

3.4.3 Superhydrophobic property of textured surfaces coated with REO

As explained previously, ceria-coated textured surfaces exhibit *superhydrophobic* Cassie wetting behavior, with a contact angle of ~ 160° and complete recoil of impacting drops. Superhydrophobic surfaces that can repel impacting water droplets require both surface texture and hydrophobic surface chemistry (exceptions to this include special re-entrant surface textures[74]). While it is well known in the literature that many metals and ceramics adsorb hydrocarbons to lower their surface energy and can show high water

CAs (typically around ~70°-80°), hydrocarbon adsorption alone is not sufficient to promote superhydrophobic properties such as Cassie-state droplets or drop bouncing. If this were possible, many of the metal/metal oxide surfaces when textured should be able to bounce water droplets off the surface -- but this does not happen and on the contrary textures often makes these materials superhydrophilic.

In this experiment, surface carbon and contact angles were compared between micro-nano textured silicon surfaces both with and without sputtered ceria coating. The textured surface used was a nanograss-covered silicon micropost surface, similar to the one in Figure 3-5 above. As can be seen in Table 3-3, the contact angles are significantly different: the ceria-coated textured surface is superhydrophobic (water droplets are in Cassie state with high contact angles ~ 160°), while the as-fabricated uncoated micro-nano textured silicon surface is superhydrophilic. As discussed previously, water droplets bounce off such ceria coated surfaces.

Table 3-3: Surface carbon (measured by XPS) and water contact angle.

Surface	**Surface carbon (%)**	**Contact angle (°)**
As-fabricated micro-nano textured silicon surface	22.2	0
Ceria-coated micro-nano textured silicon surface	15.6	160

Based on these multiple experiments that demonstrate the non-wetting properties of REO ceramics under different conditions, it can be argued that hydrocarbon adsorption exclusively cannot explain these results and leads to the conclusion that REOs are intrinsically hydrophobic.

3.5 Role of Surface Oxygen-to-Metal Ratio on the Wettability of REOs

The surface chemistry of REOs plays a significant role in determining the wettability. If the REO surface were to be modified in that the surface lattice oxygen sites were increased relative to the rare-earth metal sites, its hydrophobicity will be affected. In other words, a net increase in the surface oxygen-to-metal ratio beyond the typical stoichiometric value is detrimental because an increase in surface lattice oxygen provides more avenues for hydrogen-bonding with interfacial water which further breaks down the hydrophobic hydration structure seen in Figure 3-3, thereby increasing wettability. In the case of ceria (CeO_2) studied in this project, an O/Ce ratio higher than 2.0 can negatively impact wettability, as it provides more sites for hydrogen bonding with water.

There are many factors that could potentially cause a departure from the pristine stoichiometric state of ceria. Chin *et al.*[75] found that freshly sputter-deposited ceria films have an over-stoichiometric O/Ce ratio on the surface, reaching as high as 3.3. They attributed this anomaly to cerium vacancies or interstitial excess oxygen on the surface arising from the sputtering process. Such surfaces need to undergo long-term relaxation to reach an optimal surface stoichiometry before intrinsic hydrophobicity can be truly ascertained.

If REOs were made to relax in ambient air, atmospheric hydrocarbon contaminants would potentially accumulate on the surface and hence interfere with genuine intrinsic hydrophobicity. Hence, in order to observe surface relaxation in an environment isolated from airborne hydrocarbon contaminants, a UHV chamber that was maintained at a vacuum of $1.4 – 4.8 \times 10^{-10}$ torr was used. A 300 nm thick layer of ceria was sputter-deposited on a silicon wafer and immediately transferred in a vacuum

desiccator to the UHV chamber. *In situ* XPS analyses were conducted in the same chamber at regular time intervals for 6 hours after which the sample was left to relax in the chamber overnight for 14 hours, following which a final XPS spectrum was obtained.

Figures 3-10(a) and 3-10(b) compare the high-resolution XPS spectra for cerium (Ce 3d) obtained before and after overnight UHV relaxation respectively. It can be seen that the shape of the cerium spectrum changed considerably after overnight relaxation for 14 hours in UHV. To investigate this change in detail, the Ce 3d spectra were deconvoluted into constituent satellite peaks and identified using the nomenclature proposed by Burroughs *et al.*[76]. Specifically, the satellite peaks were designated with two different letters for the two 3d components of Ce 3d; *v* for $3d_{5/2}$ peaks and *u* for $3d_{3/2}$. All constituent satellite peaks of Ce 3d were identified by this method as shown in Figures 3-10(a) and 3-10(b) (with the exception of u_o and v_o which could not be resolved at their characteristic peak position due to lack of intensity). The peaks were fitted according to the constraint that the intensity ratio between each *v* peak and its corresponding *u* peak should equal 1.5[77,78].

The peaks were then associated with the Ce^{4+} or the Ce^{3+} oxidation state. Peaks *v*, *v″*, *v‴*, *u*, *u″* and *u‴* were associated with the Ce^{4+} state, while v_0, *v′*, u_0 and *u′* were associated with the Ce^{3+} state[76–80]. The relative concentrations of Ce^{4+} and Ce^{3+} were determined using the following equations[76–80]:

$$A(\mathrm{Ce}^{3+}) = A(v_0) + A(v') + A(u_0) + A(u')$$

$$A(\mathrm{Ce}^{4+}) = A(v) + A(v'') + A(v''') + A(u) + A(u'') + A(u''')$$

$$\% \, Ce^{y+} = \frac{A(Ce^{y+})}{A(Ce^{3+}) + A(Ce^{4+})} \times 100 \quad (y = 3, 4)$$

$A(x)$ above refers to the peak area (and corresponding peak intensity) as determined from the XPS spectra.

Using the above equations it was determined that the Ce^{3+} contribution to the overall surface cerium increased from 10.2% to 27.2% with overnight relaxation in UHV, while the Ce^{4+} contribution decreased from 89.8% to 72.8%. This indicates that the ceria sample underwent a partial reduction in state from Ce^{4+} to Ce^{3+} in UHV, which is consistent with Zhang *et al.*'s[79] observations. Specifically, it can be seen in Figures 3-10(a) and 3-10(b) that the intensity of both the characteristic Ce^{3+} peaks v' and u' increased following overnight relaxation in UHV, while the characteristic Ce^{4+} peaks v, v'', v''', u, u'' and u''' all decreased in intensity. Preisler *et al.*[81] have further correlated the change in the oxidation state from Ce^{4+} to Ce^{3+} with a net decrease in the O/Ce ratio. Therefore, in view of all these observations, it can be claimed that the change in cerium chemistry as seen in Figures 3-10(a) and 3-10(b), is consistent with the hypothesis that surface relaxation in UHV caused an overall decrease in the surface O/Ce ratio.

It can be further seen from Figures 3-10(c) and 3-10(d) that the intensity of both the lattice and non-lattice oxygen peaks decreased with overnight relaxation in UHV. It is known in literature that ceria can release surface lattice oxygen as part of a wider surface reconstruction process. As an example, Solovyov *et al.*[82] studied oxygen reconstruction on an unstable [001] ceria surface. Such surfaces release lattice oxygen in order to maintain a net zero dipole moment perpendicular to the surface, which potentially explains the reason for decreasing lattice oxygen sites as observed by the reduction in the

lattice oxygen peak intensity after overnight relaxation in UHV. Therefore, the change in the surface oxygen is consistent with the hypothesis that surface relaxation in UHV caused an overall decrease in the surface O/Ce ratio.

The non-lattice oxygen peaks at 530.7 eV and 531.4 eV in Figures 3-10(c) and 3-10(d) have been previously attributed to adsorbed surface oxygen species such as hydroxyls or carbonates[53,83,84]. Furthermore, the characteristic O 1s peak associated with adsorbed molecular water at 532.9 eV was not observed. Martínez *et al.*[53] on the contrary observed very intense peaks for adsorbed surface oxygen and molecular water relative to the lattice oxygen. Thus, the low concentration of adsorbed surface oxygen species relative to the lattice oxygen as well as the lack of adsorbed molecular water confirms the low degree of surface contamination on our ceria sample. This is attributable to the quick transfer of the sputtered samples to the UHV chamber under vacuum as well as the clean, isolated nature of the UHV environment.

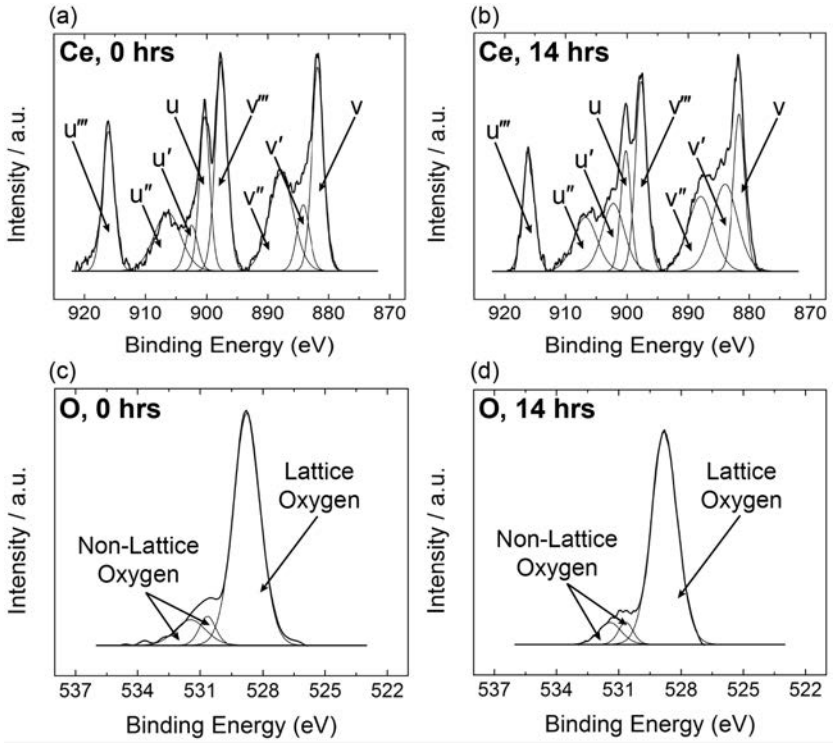

Figure 3-10: (a) XPS spectrum of cerium (Ce 3d) with constituent satellite peaks obtained immediately after loading in the UHV chamber. (b) XPS spectrum of cerium (Ce 3d) with constituent satellite peaks obtained after 14 hours relaxation in UHV. (c) XPS spectrum of oxygen (O 1s) immediately after loading in the UHV chamber. (d) XPS spectrum of oxygen (O 1s) obtained after 14 hours relaxation in UHV[85].

The high-resolution XPS spectra were used to determine the relative surface atomic concentrations of cerium, oxygen and carbon. Figure 3-11(a) shows that as the sample relaxed in UHV, the surface O/Ce ratio steadily decreased from 3.0 to 2.2 over the 14 hours of the experiment, reaching close to the stoichiometric ratio of ceria. The surface carbon remained steady at ~12% throughout the experiment as seen in Figure 3-11(b) which was expected given that the UHV chamber was practically devoid of hydrocarbon contaminants, and well sealed from the ambient environment.

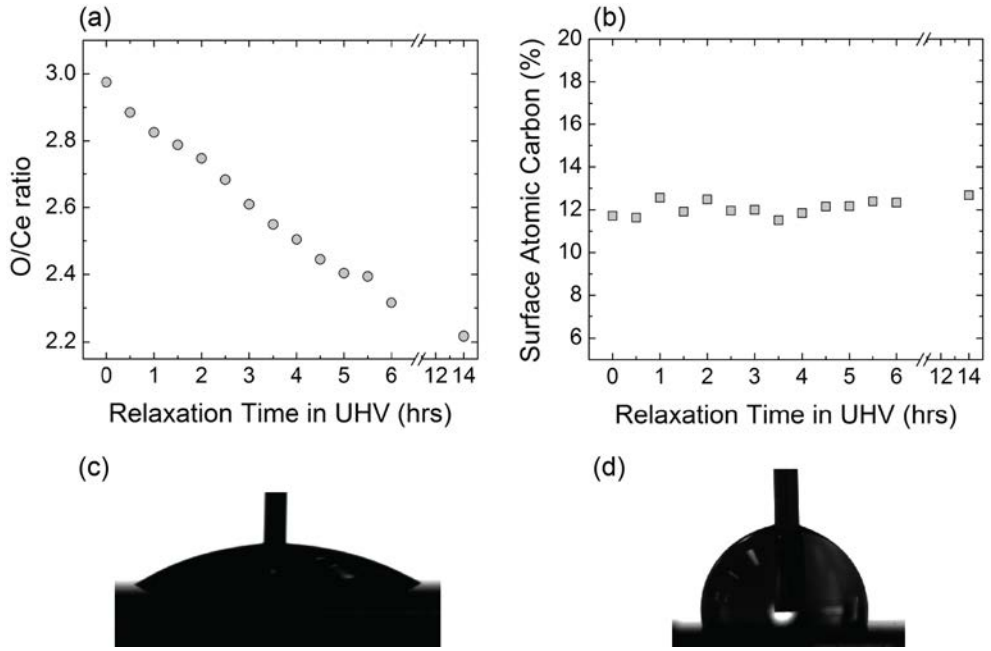

Figure 3-11: (a) Effect of UHV relaxation of a sputtered ceria surface on the O/Ce ratio. The O/Ce ratio decreases from ~3.0 at the start of the analysis to ~2.2 after 14 hours in a UHV chamber. (b) Variation of surface atomic carbon concentration with relaxation time in UHV. (c) Advancing water contact angle on a freshly-sputtered ceria surface with an O/Ce ratio of ~3.0 measured as 15° using a goniometer. (d) Advancing water contact angle on a UHV-relaxed ceria surface with an O/Ce ratio of ~2.2 measured as 104° using a goniometer.

How does the decreasing O/Ce ratio impact wettability? As explained previously in Figure 3-3, greater the oxygen sites on the surface, the greater the tendency to form hydrogen bonds with interfacial water and hence higher the wettability. As seen in Figure 3-11(a), the O/Ce ratio on a freshly sputter-deposited ceria surface was measured as ~3.0, which is similar to Chin *et al.*'s[52] observations. Indeed, it was observed that water spreads on a freshly sputter-deposited ceria surface as shown in Figure 3-11(c) given the higher-than-stoichiometric O/Ce ratio. However, when this surface was allowed to relax in a UHV environment, the O/Ce ratio approaches the stoichiometric ratio and the surface is rendered hydrophobic (WCA > 90°) as shown in Figure 3-11(d). Hence, because of the

extensive surface relaxation in the form of decreasing O/Ce ratio, the ceria surface transitioned from being initially hydrophilic to hydrophobic. It is important to note that this transition occurred with a negligible change in surface carbon content. This demonstrates that surface relaxation and determining the O/Ce ratio are crucial towards ascertaining hydrophobicity of REOs and surface hydrocarbons do not exclusively explain this unique phenomenon. This is further consistent with contact angle measurements confirming hydrophobicity on the relaxed sample with a close-to-stoichiometric O/Ce ratio, and is overall consistent with our theory on wetting behavior of REOs. Table 3-4 summarizes the results from the start and end points of the surface relaxation experiment.

Table 3-4: Comparison of water contact angles, O/Ce ratio and surface carbon content on freshly sputtered and UHV-relaxed ceria samples

Sample	**Advancing WCA (°)**	**O/Ce ratio**	**Surface Carbon (%)**
As-sputtered	15 ± 6	2.98 ± 0.04	11.7 ± 0.3
UHV-relaxed (14 hours)	104 ± 3	2.22 ± 0.02	12.7 ± 0.2

This experiment shows how excess surface oxygen can negatively impact hydrophobicity of REOs. More broadly, it is shown that surface chemistry (in particular, excess surface oxygen) and surface relaxations can impact wettability of REOs. In fact, contact angle measurements can be used as a tool to determine the extent of surface relaxation of REOs. It is important to carefully consider these effects before ascertaining the true origins of hydrophobicity of REOs.

3.6 Drawbacks of Hydrocarbon Contamination Cleaning Methods

Given the interference of airborne hydrocarbon contaminants, wettability studies on REOs should be ideally performed on hydrocarbon-free surfaces. However, some of the known hydrocarbon cleaning approaches applied to REOs have inherent drawbacks in that they either alter the pristine surface chemistry of REOs or introduce morphological defects *concurrently* with hydrocarbon removal, and thereby affect wettability. The following cleaning methods in particular have been investigated in detail: plasma cleaning, thermal annealing, UV radiation treatment and thermal annealing.

Argon plasma etching is a well-known method to clean surfaces, however it has been shown to disturb the pristine surface chemistry of REOs. In the case of ceria, cleaning by argon plasma induces polarized oxide groups on the surface, which in turn results in increased hydrogen bonding with water and hence increased wettability[86]. Similarly, ultraviolet (UV) radiation treatment of ceria introduces hydrophilic superoxide species on the surface, which are not easily removed in vacuum and can lead to lowering of contact angle[87–89].

Thermal annealing as an approach to burn off surface hydrocarbons is also disadvantageous as it can introduce cracks and other severe morphological defects that consequently impact wettability. In thin ceramic films in particular, there is often a significant co-efficient of thermal expansion (CTE) mismatch between the film and the underlying substrate, which can further accentuate the formation of cracks and defects upon annealing and expose areas of the underlying substrate. In terms of the implications of these defects on wettability, it is well known that chemical heterogeneities can affect contact angle measurements and result in pinning sites[4,57,90]. Hence, contact angle

measurements are *unpredictable* and *unreliable* on annealed thin films that have defects and exposed areas of the underlying substrate.

Morphological defects broadly refer to cracks and pits and other structural shortcomings on the surface that can interfere with wettability measurements. As such, if an REO surface is ridden with cracks and defects and contact angle measurements it can be falsely construed as hydrophilic. To demonstrate such defects, foils of Gadolinium and Dysprosium metal were annealed at 500°C. The annealing process automatically resulted in the formation of an oxide film on the surface. However, as shown in Figure 3-12, the thermal annealing processes resulted in surfaces that are covered in defects and cracks at both macroscopic and microscopic length scales. The annealed surface is quite unstable, flaky, and spalls off the surface to expose the underlying metal (Figure 3-12). These cracks and surface defects can provide pathways for water to hemi-wick, spread on the surface, and also come into contact with the underlying reactive metal. Hence, water contact angle measurements on annealed surfaces will be significantly affected by a combination of hemi-wicking at the defect sites and possible reaction with the underlying metal.

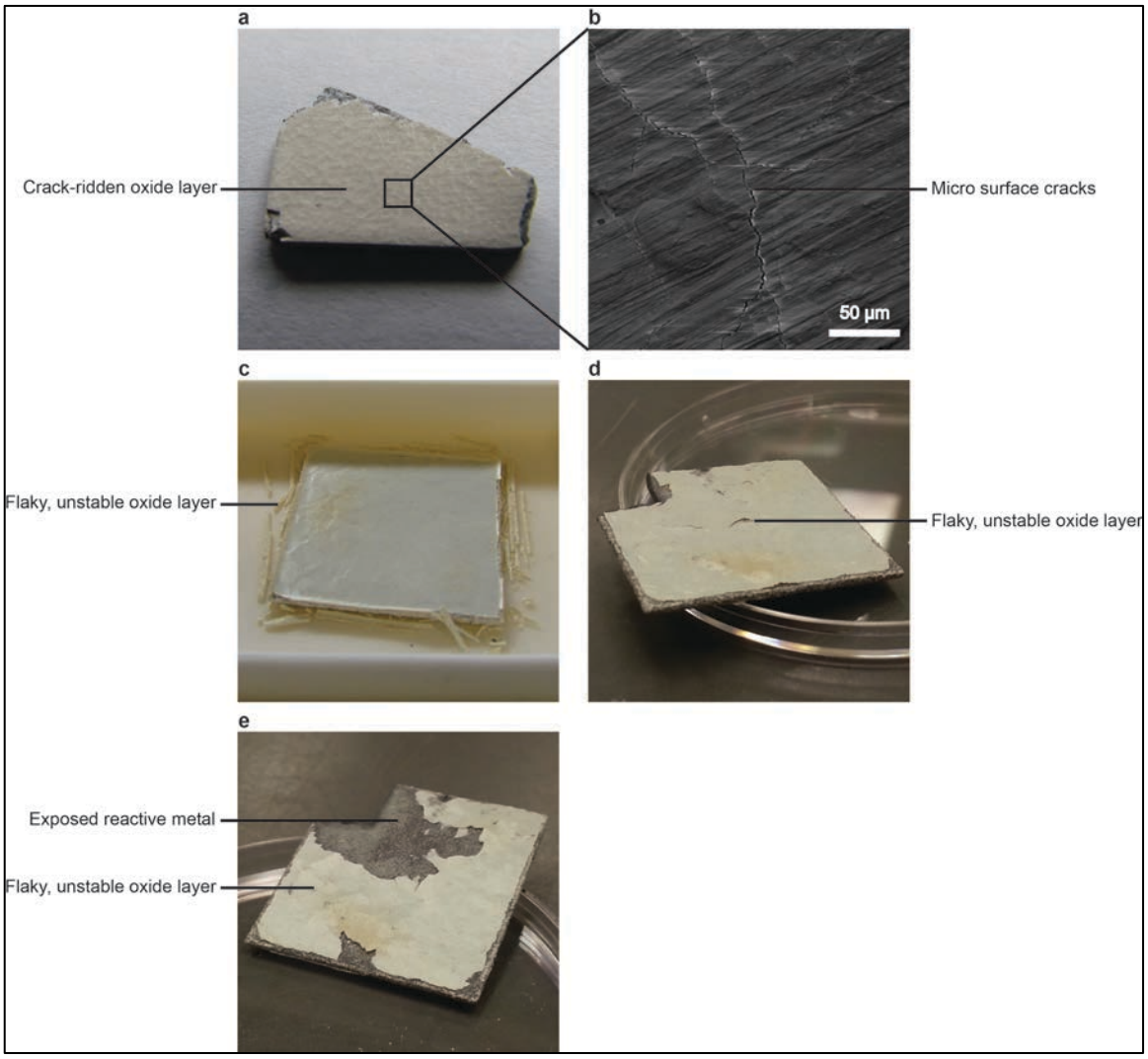

Figure 3-12: Morphology of annealed surfaces (a-b) visible cracks on the Gd surface as well as microcracks at higher magnification (c-e) flaky oxide layer on annealed Dy surface

To demonstrate the formation of morphological defects from CTE mismatch, ceria-coated silicon wafers were annealed at 500°C for 1 hour. One of these wafers was then cooled down to room temperature and then again annealed at 500°C for another hour. In both cases, it was found that the annealing process introduced severe morphological defects on the surface. After analyzing the samples under SEM, ubiquitous pits were found on the surface revealing the underlying hydrophilic silicon substrate (see Figure 3-13(a)). In fact in the goniometer images in Figure 3-13(b) we can

clearly see hydrophilicity due to these defects, and that the contact angle is unequal on both sides of the drop due to the apparent pinning by these defects, in agreement with past literature[4,57,90]. Hence, if contact angle measurements, it would lead to false conclusions about the hydrophobicity of REOs.

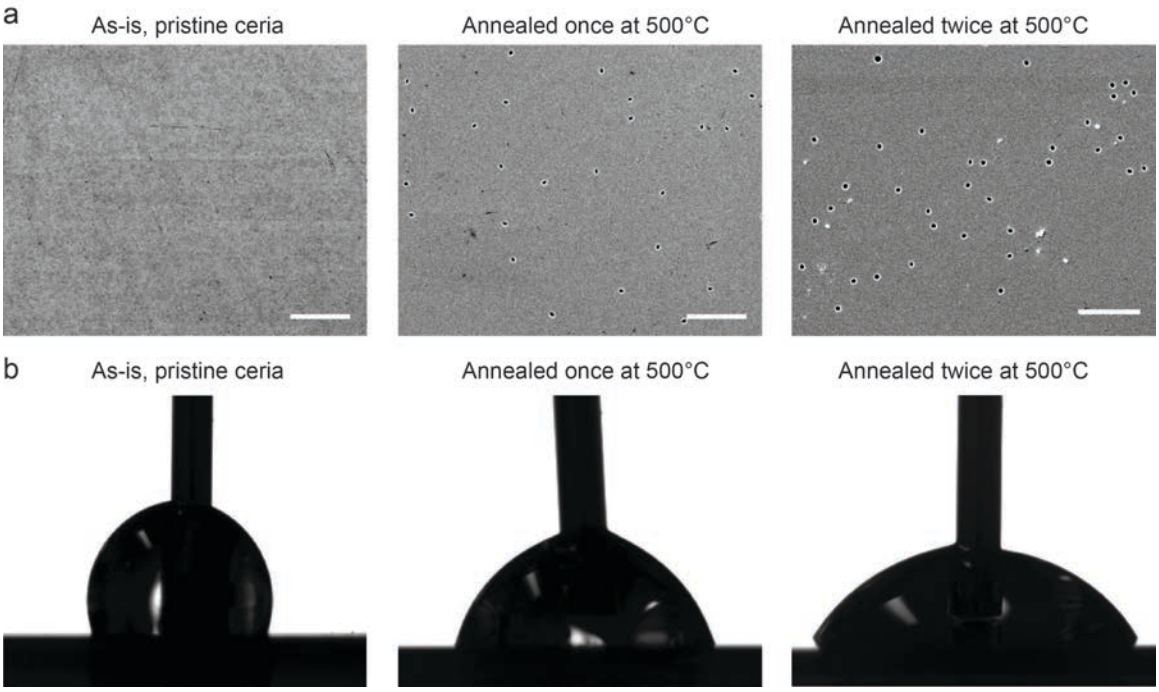

Figure 3-13: (a) Scanning electron microscopy (SEM) images of ceria samples (Scale bar: 50 μm). Pits and defects can be clearly seen in the samples annealed at 500°C (b) Water contact angle (WCA) measurements on ceria samples using a goniometer

To demonstrate that removal of hydrocarbon contamination from annealing *exclusively* does not explain the reduction in contact angle post annealing, the above annealed samples were exposed to ambient air for about four weeks and then the surface hydrocarbon content was measured. As seen in Table 3-5, the ceria sample annealed at 500°C and left in ambient air for four weeks had a surface carbon content of ~35% (which is similar to previously reported carbon content on hydrophobic REOs exposed to ambient air for extended time periods[73]). *Yet,* it was found that this annealed sample was

hydrophilic with a contact angle of 69°. If surface carbon were to be the *sole factor* causing hydrophobicity in REOs, then the ceria sample annealed at 500°C should have been hydrophobic after exposure to ambient air for such an extended period and having an over 50% higher surface carbon level than that reported previously. In fact, the surface carbon content on the annealed sample was almost *three times* higher than the carbon content observed in our recent paper on a relaxed, hydrophobic ceria surface[85] and yet it was hydrophilic. This clearly demonstrates that the major morphological defects induced by the annealing process reduce the hydrophilicity of REOs rather than surface hydrocarbon contamination, and that there is no direct correlation between hydrophobicity of REOs and surface carbon content.

Table 3-5: Comparison of Surface Carbon Content and Water Contact Angle on Ceria Samples

Surface	**Surface carbon (%)**	**Advancing Contact angle (°)**
1. Ceria, as is, relaxed and pristine	12.7%	104
2. Ceria sample annealed at 500°C for 1 hour and left in air for ~4 weeks	32.8%	68
3. Ceria sample sputtered *in situ* with Ar+ in XPS chamber and allowed to relax overnight in UHV	4.2%	96

Therefore, if any of the above cleaning methods were to be used on REOs, it would alter the pristine hydrophobic state, which should be taken into consideration while ascertaining wettability of REOs.

3.7 Hydrophobicity at Ultra-low Surface Carbon Levels

Finally, to demonstrate that REOs possess intrinsic hydrophobicity even at ultra-low surface carbon levels, Ar^+ ions were sputtered on a ceria sample *in situ* within a UHV chamber (measured carbon after sputtering was <1%), and the sample was allowed

to relax overnight for 12 hours in the same chamber (in order to let the sample reach an optimal chemistry and consequent hydrophobic state post-relaxation) and then the water contact angle was immediately measured. It was observed that indeed the sample was hydrophobic with a contact angle of 96°, even though the surface carbon was only 4.2%. This demonstrates that when free from any detrimental morphological or surface chemistry defects, REOs possess an element of intrinsic hydrophobicity *even at extremely low surface carbon levels.*

In summary, in view of all of the above results, it can be conclusively confirmed that *rare-earth oxides are intrinsically hydrophobic*. Airborne hydrocarbon contaminants do not exclusively explain the hydrophobicity of REOs, and standard cleaning methods to remove surface hydrocarbon contamination introduce chemical and/or morphological defects simultaneously that affect wettability. The lowering of contact angle on ceria after annealing cannot be *exclusively attributed* to removal of surface hydrocarbon, *but rather* to the *severe morphological defects* introduced by the process. Saturating these samples with more hydrocarbons does not change wettability, and we have also demonstrated that REOs are intrinsically hydrophobic even at ultra-low carbon levels.

Hydrophobicity of REOs continues to be an evolving area of research around the world, as well as at MIT. The following recent independent studies additionally support intrinsic hydrophobicity of REOs[91–93].

4. Sustained Dropwise Condensation on REOs

Given that REOs possess intrinsic hydrophobicity, it is worthwhile investigating viable long-term applications. As explained earlier, dropwise condensation is a field that has been researched quite extensively over the past several decades, but has been difficult to realize in industrial applications given that most hydrophobic materials deteriorate in harsh steam conditions, or installing them is simply not cost-effective. It is hypothesized that REOs will demonstrate sustained long-term dropwise condensation with their robustness and longevity. This chapter will present results from an accelerated condensation study on thin-film coatings of REOs.

4.1 Need for a Titanium Adhesion Layer

The stability of rare earth oxides on metals has been a subject of research for many years[94–98]. Metals are widely used in industrial applications and are prone to issues such as corrosion and scale-formation[94,95]. Some metals such as copper and nickel are unable to maintain a stable REO film when subject to harsh conditions such as high temperature. Furthermore, current literature shows no evidence of past work of REO coatings on titanium. In this study, proof-of-principle stability of REO coatings on titanium using ceria has been demonstrated (see Figure 4-1 for schematic of the proposed titanium adhesion layer).

Figure 4-1: Cross-section view of a ceria film deposited on titanium on a silicon substrate

A 90 nm thin layer of titanium was sputter-deposited on a silicon wafer after which further on this layer, a ~300 nm layer of ceria was deposited. Figure 4-2 shows a cross-section of the two layers deposited as seen under an SEM.

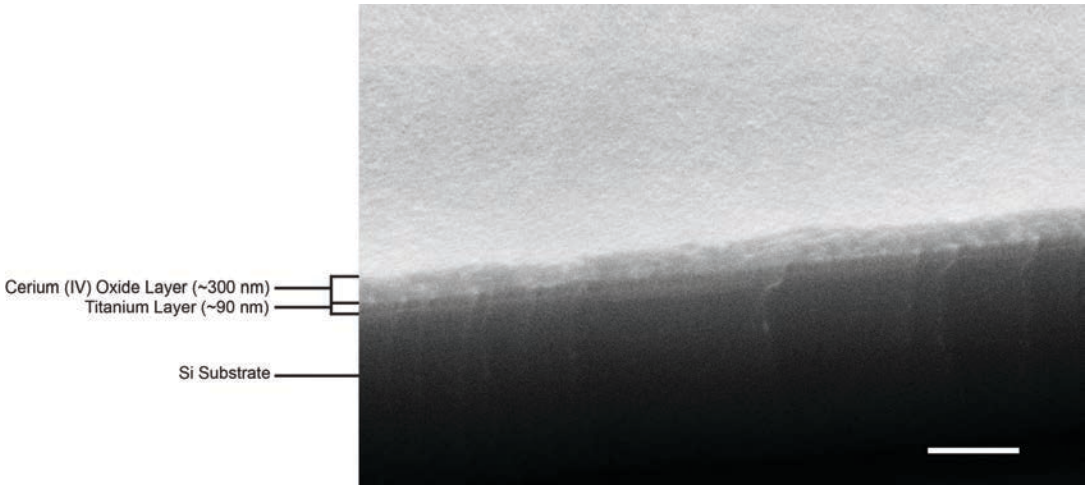

Figure 4-2: SEM Micrograph image showing cross section of the cerium oxide layer deposited on top of a titanium adhesion layer on a silicon substrate. Scale bar: 1 μm.

In order to test the stability of wafers coated with the films as shown above in Figures 4-1 and 4-2, these wafers were subject to two harsh processing conditions: steam treatment and boiling, both for one hour. For the sake of comparison, ceria films deposited on the wafers in the absence of the titanium layer were also studied.

As seen in Figure 4-3 (a), steam treatment caused damage to the ceria coating deposited in the absence of a titanium layer, thereby revealing the underlying substrate. However, as seen in Figure 4-3 (b), ceria in the presence of the titanium adhesion layer did not degrade despite the steam treatment. In fact, the ceria layer did not wear off even after 100 hours of continuous steam treatment (details of this experiment are in Sections 4.2 and 4.3).

The sample was then immersed in a 250 ml beaker containing boiling water

maintained at 100°C for one hour. Similar damage and flaking was observed on the ceria sample without the titanium adhesion layer after boiling water treatment as seen in Figure 4-3 (c). However, in contrast, the ceria films coated on the titanium adhesion layer show superior robustness with no visual signs of damage to the coating after treatment with steam or boiling water, as seen in Figures 4-3 (b) and (d) respectively.

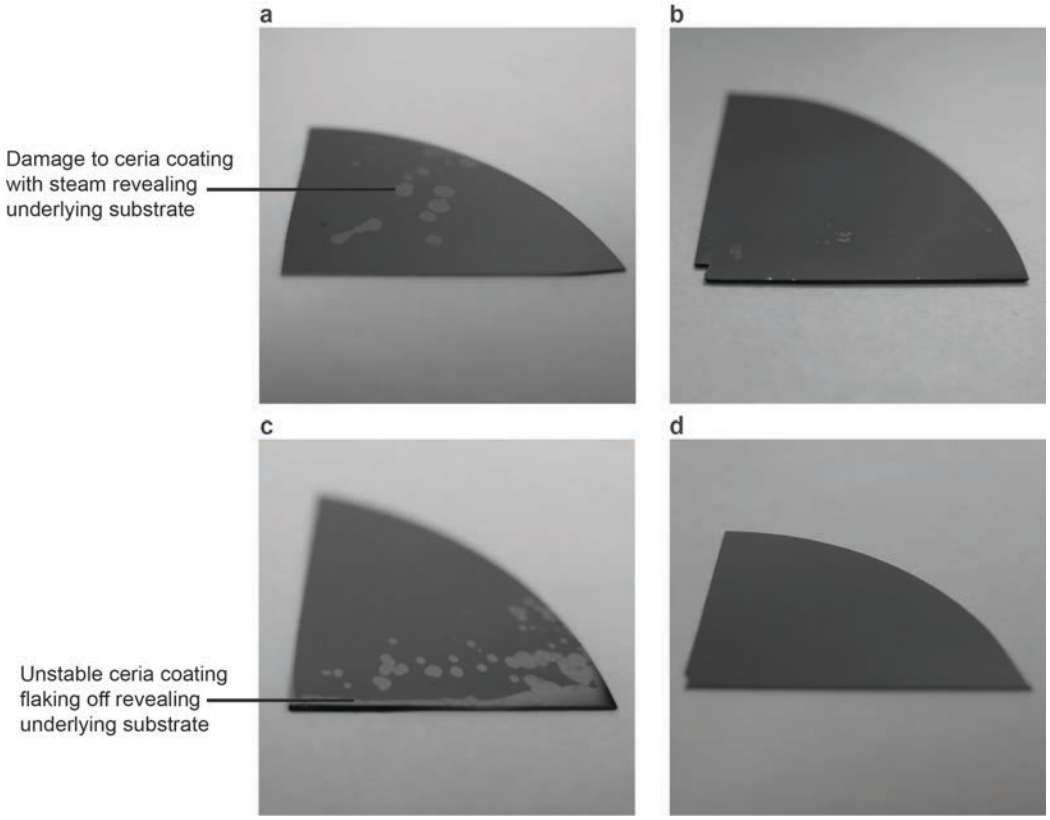

Figure 4-3: (a) Ceria film in the absence of an underlying titanium layer exposed to steam for 1 hour (b) Ceria film with an underlying titanium layer exposed to steam for 1 hour (c) Ceria film in the absence of an underlying titanium layer exposed to boiling water for 1 hour (d) Ceria film with an underlying titanium layer exposed to steam for 1 hour

No previous reported metal possesses the advantage of adhering to a stable REO coating than titanium. This work is the first to report the potential longevity of REO

coatings in the presence of titanium especially when subjected to destructive conditions such as steam and boiling water. In the presence of titanium, hydrophobic REO coatings can outperform other hydrophobic materials such as organic silanes that would normally degrade relatively quickly in the presence of harsh process environments

Particular advantage can be seen in the hydropower industry and marine applications where hydrophobic REOs in the presence of titanium can maintain integrity and promote corrosion resistance for an extended period of time. As addressed previously, these materials also have anti-scaling and bio-fouling resistant properties owing to their low surface energy. Environmental damage that is commonly associated with degradation of process equipment and coatings either due to corrosion or harsh process conditions will be extremely minimized given the robustness and longevity promise of these adhesion layers.

4.2 Experimental Rig for Steam Condensation Experiments

The experimental rig used for accelerated steam condensation experiments in this project was designed by Adam T. Paxson[99] – see Figure 4-4 for schematic of the rig set-up and photographs.

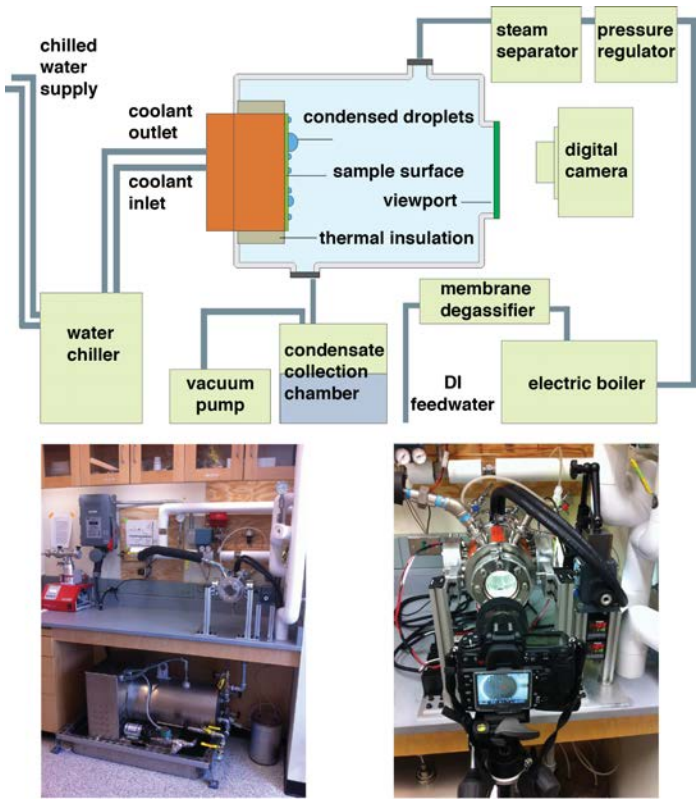

Figure 4-4: Schematic of condensation rig and photographs

4.2.1 Accelerated Steam Conditions

In general, surface condensers in power plants operate under sub-atmospheric vacuum conditions in order to lower the temperature required to condense which is determined from the thermodynamic properties of saturated steam. The effects of non-condensable gases in the measurements in particular must be given special consideration, as it could lead to inaccurate measurements. The main condensation chamber shown in Figure 4-4 is held under vacuum in order to replicate the conditions of a typical industrial condenser. Typical operating pressures and temperatures of power plant condensers are between 3 and 5 kPa and 25 and 30°C [99].

However, for the purpose of this project, a significantly higher operating pressure and temperature of saturated steam was chosen and employed in the condensation test rig

chamber – 90 kPa and 97°C respectively; for two reasons. Firstly, such higher temperatures and pressures best represent *harsh steam conditions* -- and if REOs are indeed able to survive under these conditions and maintain hydrophobicity and integrity, they provide meaningful implications on the long-term robustness of these coatings. Secondly, these conditions are able to shorten the duration of endurance tests. In other words, if the REO coatings do not degrade after 100 hours of condensation at the harsh steam conditions of 90 kPa and 97°C, it can be predicted with reasonable confidence that they would be sustainable for a significantly longer time, likely in the order of years, at the relatively more benign conditions in typical power plants -- which as stated earlier are significantly less harsh at around 3 kPa and 25°C respectively.

4.2.2 Measurement Principle of Heat Transfer Co-efficient

This condensation chamber enables direct measurement of the heat flux over a wide range of experimental conditions, analogous to those of real industrial condensers. In order to measure the heat transfer co-efficient, the philosophy shown in Figure 4-5 was employed.

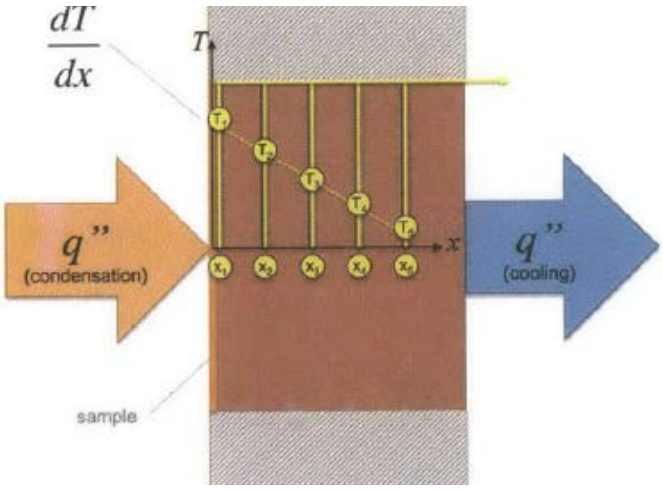

Figure 4-5: Measurement philosophy of the heat transfer co-efficient employed in the condensation test rig used in this experiment[99]

A sample-cooling block (or "puck") made of titanium or copper (shown above in brown) has a few drilled holes for inserting highly accurate temperature measuring devices called thermistors (accuracy of ±0.01°C). These instruments measure temperatures T_1 to T_n at sample points x_1 to x_n in the puck. The sample side of the puck (left side in Figure 4-5) is exposed to saturated steam while the back-side is cooled. Thermal insulation around the periphery of the block ensures one-dimensional heat transfer, so that all heat fluxes occur in parallel. As such, the thermal temperature gradient, dT/dx can be calculated from the thermistor measurements, and the surface temperature T_s can be extrapolated. Further, knowing the thermal conductivity of the puck material k, the heat flux q can be calculated using Fourier's law:

$$q = -k\frac{dT}{dx} \qquad \text{Equation 4.1}$$

Once the heat flux q and the surface temperature T_s have been determined as above, knowing the saturated steam temperature T_{sat}, the condensation heat transfer co-efficient h can be calculated using:

$$h = \frac{q}{T_s - T_{sat}} \qquad \text{Equation 4.2}$$

In these experiments, saturated steam at a pressure of 90 kPa and temperature of 97°C was generated by a 20 kW electric boiler. A water-cooled heat exchanger provided 20 kW of cooling power to the test surface. The heat flux and heat transfer co-efficient were measured by calculating the temperature gradient along the cooling block as described above, and the departing drop sizes were measured from images obtained with a high-resolution Nikon D300 video camera. Non-condensable gases were constantly purged from the space right in the vicinity of the sample surface using a vacuum vent.

This rig also has integrated control features that can maintain the saturation pressure and temperature of the steam. Furthermore, endurance features have been implemented to replenish water in the boiler so that the rig can be operated indefinitely for endurance purposes. As stated previously, all of the condensation experiments were conducted continuously for 100 hours under accelerated steam conditions and were made possible by these endurance features.

4.3 Condensation on Ceria

To study condensation of steam on ceria, a thin-film (~300 nm) of ceria was sputter-deposited on a 90 nm titanium layer on a silicon wafer using the technique described in Section 4.1. Using Atomic Force Microscopy (AFM), the mean root mean square (RMS) roughness of the sample was determined to be 34 ± 6 nm (See Figure 4-6). The advancing and receding contact angles on the sample were measured to be 102° and 74° respectively. The wafer was then clamped to an instrumented titanium puck and fitted inside the condensation chamber as seen in Figure 4-6 (b).

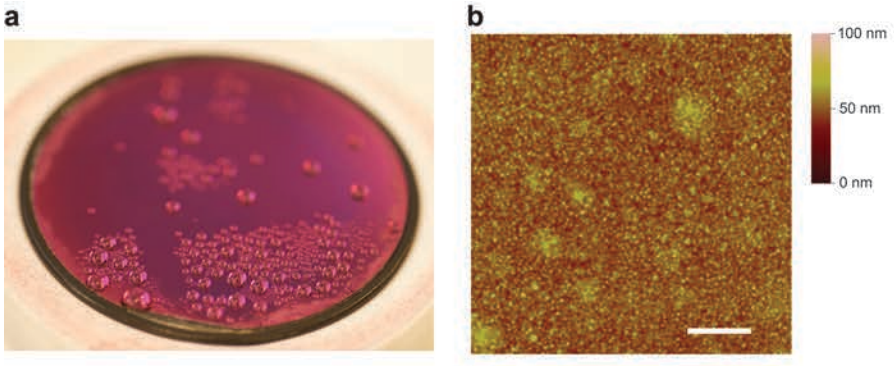

Figure 4-6: Condensation on ceria. a) A ~300 nm layer of ceria deposited on a ~90 nm layer of titanium on a silicon wafer that was then attached to a titanium puck and fitted inside the condensation chamber. b) AFM micrograph of the ceria sample showing a highly smooth surface with an RMS roughness of 34 ± 6 nm

Steam was then introduced in the chamber and it started condensing on the ceria sample. As seen in Figure 4-7, excellent dropwise condensation behavior was observed on the sample and was maintained throughout the 100 hours duration of the experiment. No significant degradation of the ceria film was observed throughout the experiment, and the film retained its hydrophobicity throughout.

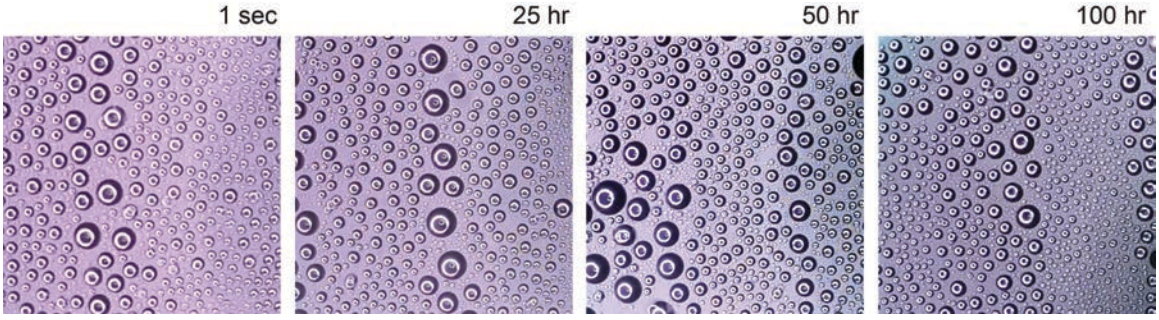

Figure 4-7: Sustained dropwise condensation on ceria for 100 hours

Using the heat transfer co-efficient calculation principle described earlier, the heat transfer co-efficient on ceria was calculated to be 107 ± 5 kW/m^2K. This is an almost tenfold improvement in previously reported heat transfer co-efficient values on hydrophilic materials such as aluminum (<10 kW/m^2K)[24,42,100]. This demonstrates the excellent advantage of using hydrophobic ceria coatings in maintaining dropwise condensation and ensuring superior heat transfer performance.

4.4 Condensation on Erbia

The 100 hours steam condensation experiment with ceria above demonstrated long-term robustness of ceria that was coated on a silicon wafer. However, commercial condensers are typically constructed using metals such as titanium, stainless steel, copper, and aluminum. To demonstrate realistic performance on such a relevant industrial material as well as versatility within the REO series, another REO erbia was directly sputter-deposited on a titanium puck as shown in Figure 4-8 (a). Using AFM, the mean

root mean square (RMS) roughness of the sample was determined to be 796 ± 128 nm (See Figure 4-8 (b)). This indicates that the sample is significantly rougher than the silicon wafer used for condensation on ceria, and is expected given the more machined finish of the titanium puck. The advancing and receding contact angles on the sample were measured as 98° and 59° respectively.

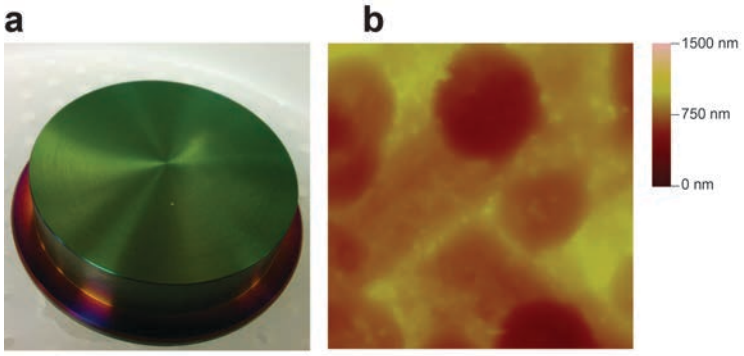

Figure 4-8: Condensation on erbia. a) A ~300 nm layer of erbia directly sputter-deposited on a titanium puck and fitted inside the condensation chamber. b) AFM micrograph of the erbia-coated titanium sample showing a rough surface with an RMS roughness of 796 ± 128 nm

Similar to ceria, sustained drop-wise condensation was observed on the erbia sample for the 100 hour duration of the experiment, as seen in Figure 4-9. The departing droplet sizes observed were significantly higher than ceria, which is expected given the higher roughness of the titanium puck as measured by AFM.

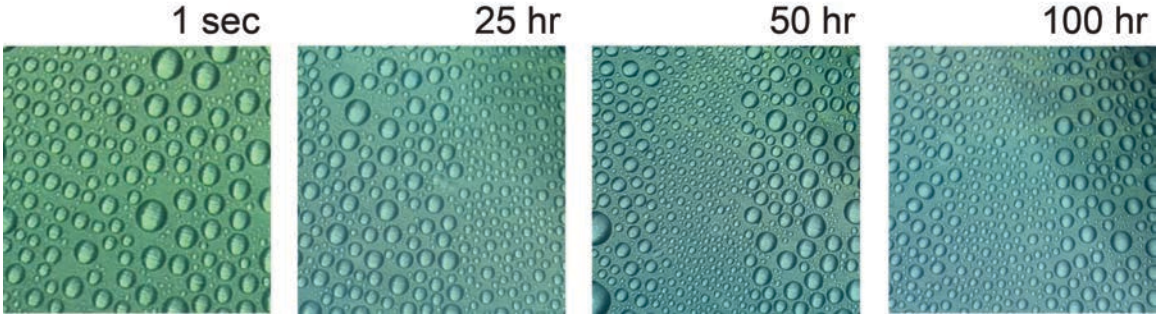

Figure 4-9: Sustained dropwise condensation on erbia for 100 hours

The heat transfer co-efficient on this sample was calculated to be 53 ± 2 kW/m^{2}K, which is again a significant improvement over heat transfer co-efficients obtained from filmwise condensation (<10 kW/m^{2}K). The heat transfer co-efficient is lower than ceria, and is expected given the greater roughness of the sample and also the greater contact angle hysteresis leading to larger size of the departing drops.

4.5 Environmental SEM Condensation

The heat transfer co-efficient from dropwise condensation also depends on density of nucleation sites on which water vapor condenses to liquid droplets[101,102]. In order to better understand the condensation process on a micro-scale, a small 2mm by 2mm chip of the ceria-coated silicon wafer was subject to condensation in an environmental scanning electron microscope (EVO 55, Zeiss). The sample was secured to an aluminum stud with double-sided carbon adhesive tape, which was then clamped into a Peltier cooling stage attached in the microscope.

The chamber was purged with water vapor three times up to 3 kPa and down to 10 Pa to remove non-condensable gases. After purging, the pressure was held at ~1000 Pa and the temperature was slowly decreased at a rate of 0.5 K min^{-1} until formation of observable water droplets (condensing from the water vapor introduced into the chamber). Accelerating voltage was kept at 25 kV and the beam current was 200 nA. Images were recorded at approximately 1-2 Hz and the stage was moved to different areas to avoid charging effects on nucleation. Figure 4-10 shows the top and side view of the condensing drops on the ceria surface.

The nucleation density was calculated using five different micrographs obtained from the environmental SEM, and was determined to be 335 ± 23 mm^{-2}. This value is on

the same order of magnitude as previously reported nucleation densities on other hydrophobic materials[24,101].

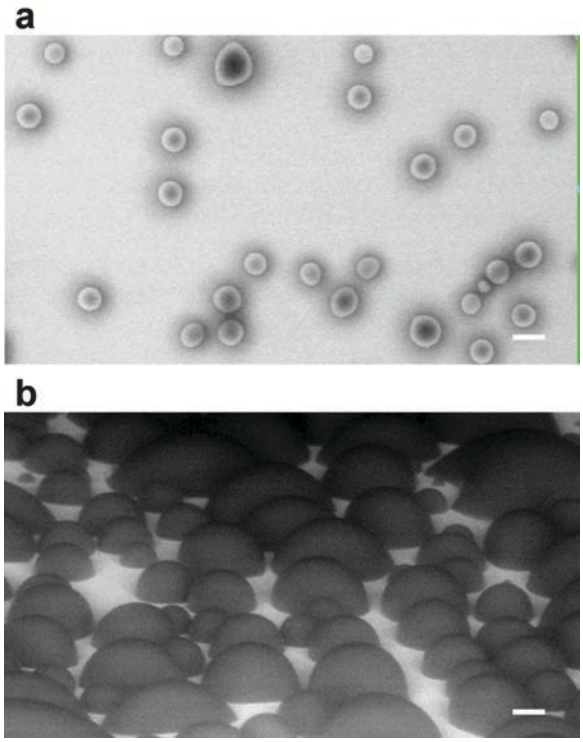

Figure 4-10: Condensing droplets on a ceria surface as seen under an environmental SEM a) top view and b) side view. Scale bars in both figures: 10 μm

4.6 Robustness of REO coatings compared to other hydrophobic coatings

As a comparison, condensation behavior on fluorosilane – a hydrophobic modifier – was surveyed from past work[24]. Although initially fluorosilane coated on a silicon wafer demonstrates dropwise condensation with a heat transfer co-efficient of 61 ± 2 kW/m^2K, it quickly degrades in a matter of minutes and exhibits filmwise condensation with a heat transfer co-efficient of 4.6 ± 0.4 kW/m^2K (see Figure 4-11)[24]. In contrast, REO coatings demonstrate outstanding versatility and robustness.

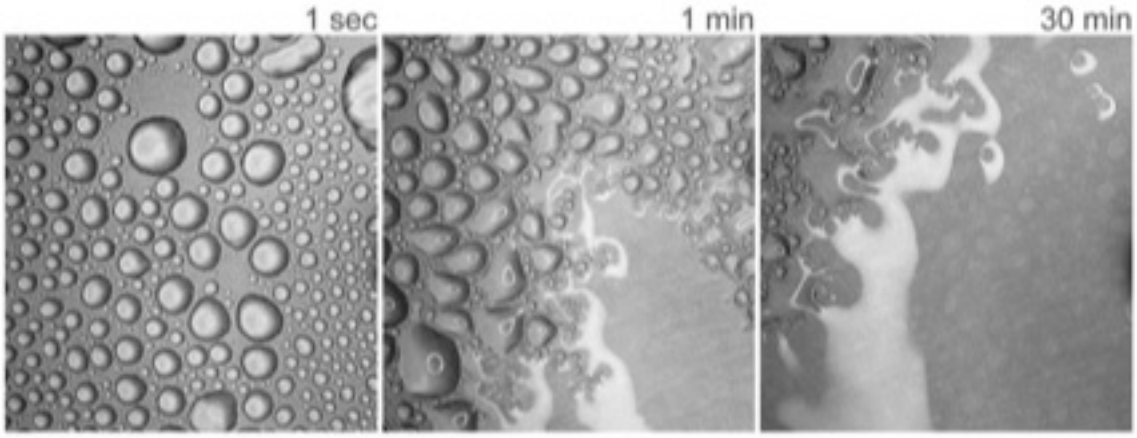

Figure 4-11: Degradation of a hydrophobic fluorosilane coating over a period of 30 min of steam condensation indicating lack of robustness compared to REOs[24]

These results clearly show that hydrophobic REOs are extremely promising as coatings in steam condensers in power plants. They do not compromise structural integrity as demonstrated by the endurance test and show a significant improvement in heat transfer performance. As addressed previously, an order of magnitude enhancement in the heat transfer co-efficient can translate into a 5-7% improvement in the overall process efficiency of steam power plants, and consequently significantly lower fuel consumption and greenhouse gas emissions.

Given that steam is a harsh environment, these results also demonstrate that REOs can be reliably used as coatings in other applications such as reducing bio-fouling and corrosion in hydropower systems.

5. Summary and Conclusions

In conclusion, hydrophobic rare-earth oxide (REO) coatings present an attractive multi-dimensional package of enhancements for the hydropower industry as well as in steam power plants. These benefits include bio-fouling resistance, drag reduction, corrosion resistance, and overall, a reliable, long-term form of protection. Further research would need to evaluate the long-term capital and operating costs in more detail and justify benefits for a typical plant, as well as prove longevity and versatility of applications. These coatings can be retrofitted in existing systems or applied in new plants, and should be considered by hydropower facilities in the overall scheme of infrastructure modernization. More specifically, the main conclusions from this research are:

- REOs are intrinsically hydrophobic, and airborne hydrocarbons that may accumulate on their surface do not exclusively explain their hydrophobicity
- The presence of excess hydrogen-bonding sites such as a higher-than-stoichiometric lattice oxygen content affects the wettability of REOs
- Surface chemistry (in particular, excess surface oxygen) and surface relaxations can impact wettability of REOs. In fact, contact angle measurements can be used as a probe to determine the extent of surface relaxation of REOs.
- Thin films of REOs demonstrate sustained dropwise condensation for over 100 hours at accelerated steam conditions without compromising structural integrity and hydrophobicity
- The resulting heat transfer co-efficients by using REO coatings are an order of magnitude higher than typical film-wise condensation

- In view of the accelerated steam condensation results, it can be predicted that REO coatings will demonstrate long-lasting hydrophobic performance in typical condensers in power plants which operate at significantly less harsh pressure and temperature conditions than the ones used in the accelerated tests in this project
- The enhancement in heat transfer performance by using hydrophobic REO coatings in turn translates to a superior improvement in the overall plant efficiency by a remarkable 3-5% and significant reduction in greenhouse gas emissions
- REOs are robust and can withstand harsh conditions and maintain their hydrophobicity and longevity in a wide variety of applications such as coatings for hydropower systems
- Despite the name "rare", in fact REOs are relatively cheap and readily available compared to other hydrophobic materials (especially ceria)

Below is the list of all publications, patents and presentations from this work:

Journal Papers

- **Khan S**., Azimi G., Yildiz B., Varanasi K. K., *Role of surface oxygen-to-metal ratio on the wettability of rare-earth oxides*, Applied Physics Letters, **106,** 061601 (2015)
- **Khan S.**, Azimi G., Paxson A., Khalil K., Varanasi K. K, *Sustained drop-wise condensation on rare-earth oxide ceramics*, Advanced Materials (submitted) (2015)

Conference Talks

- **Khan S**., World Hydropower Congress in Beijing, China (May 2015)

- **Khan S**., ACS Colloids Conference in Pittsburgh, Pennsylvania (June 2015)
- **Khan S**., ASME Interpack Conference in San Francisco, California (July 2015)
- **Khan S**., Hydrovision International in Portland, Oregon (July 2015)

Patents

- **Khan S.,** Azimi G., Paxson A., Varanasi K. K., *Improving Longevity of Rare-earth Oxide Coatings* (U.S. Patent Application Filed on October 30th, 2014 and assigned US serial number 14/528,799)
- **Khan S.,** Azimi G., Varanasi K. K., *Hydrogen-bonding Sites and Surface Oxygen Content that Impact Wettability of Rare-earth Oxides* (U.S. Patent Application Filed on January 30th, 2015 and assigned US serial number 62/109,690)

References

1. Bird, J. C., Dhiman, R., Kwon, H.-M. & Varanasi, K. K. Reducing the contact time of a bouncing drop. *Nature* **503,** 385–388 (2013).
2. Gennes, P.-G. de, Brochard-Wyart, F. & Quere, D. *Capillarity and Wetting Phenomena: Drops, Bubbles, Pearls, Waves*. (Springer Science & Business Media, 2004).
3. Butt, H.-J., Graf, K. & Kappl, M. *Physics and Chemistry of Interfaces*. (John Wiley & Sons, 2006).
4. Quéré, D. Wetting and Roughness. *Annu. Rev. Mater. Res.* **38,** 71–99 (2008).
5. Bocquet, L. & Lauga, E. A smooth future? *Nat. Mater.* **10,** 334–337 (2011).
6. Deng, X., Mammen, L., Butt, H.-J. & Vollmer, D. Candle Soot as a Template for a Transparent Robust Superamphiphobic Coating. *Science* **335,** 67–70 (2012).
7. Quéré, D. Non-sticking drops. *Rep. Prog. Phys.* **68,** 2495–2532 (2005).
8. Papadopoulos, P., Mammen, L., Deng, X., Vollmer, D. & Butt, H.-J. How superhydrophobicity breaks down. *Proc. Natl. Acad. Sci.* **110,** 3254–3258 (2013).
9. Richard, D., Clanet, C. & Quéré, D. Surface phenomena: Contact time of a bouncing drop. *Nature* **417,** 811–811 (2002).
10. Antonini, C., Amirfazli, A. & Marengo, M. Drop impact and wettability: From hydrophilic to superhydrophobic surfaces. *Phys. Fluids 1994-Present* **24,** 102104 (2012).
11. Dash, S., Alt, M. T. & Garimella, S. V. Hybrid Surface Design for Robust Superhydrophobicity. *Langmuir* **28,** 9606–9615 (2012).

12. Antonini, C., Bernagozzi, I., Jung, S., Poulikakos, D. & Marengo, M. Water Drops Dancing on Ice: How Sublimation Leads to Drop Rebound. *Phys. Rev. Lett.* **111,** 014501 (2013).

13. De Ruiter, J., Lagraauw, R., van den Ende, D. & Mugele, F. Wettability-independent bouncing on flat surfaces mediated by thin air films. *Nat. Phys.* **11,** 48–53 (2015).

14. Meuler, A. J. *et al.* Relationships between Water Wettability and Ice Adhesion. *ACS Appl. Mater. Interfaces* 101015091058040 (2010). doi:10.1021/am1006035

15. Lee, H., Alcaraz, M. L., Rubner, M. F. & Cohen, R. E. Zwitter-Wettability and Antifogging Coatings with Frost-Resisting Capabilities. *ACS Nano* **7,** 2172–2185 (2013).

16. Boreyko, J. B. & Collier, C. P. Delayed Frost Growth on Jumping-Drop Superhydrophobic Surfaces. *ACS Nano* **7,** 1618–1627 (2013).

17. Eberle, P., Tiwari, M. K., Maitra, T. & Poulikakos, D. Rational nanostructuring of surfaces for extraordinary icephobicity. *Nanoscale* **6,** 4874 (2014).

18. Maitra, T. *et al.* On the Nanoengineering of Superhydrophobic and Impalement Resistant Surface Textures below the Freezing Temperature. *Nano Lett.* **14,** 172–182 (2014).

19. Lv, J., Song, Y., Jiang, L. & Wang, J. Bio-Inspired Strategies for Anti-Icing. *ACS Nano* **8,** 3152–3169 (2014).

20. Patankar, N. A. Supernucleating surfaces for nucleate boiling and dropwise condensation heat transfer. *Soft Matter* **6,** 1613 (2010).

21. Dietz, C., Rykaczewski, K., Fedorov, A. G. & Joshi, Y. Visualization of droplet departure on a superhydrophobic surface and implications to heat transfer enhancement during dropwise condensation. *Appl. Phys. Lett.* **97,** 033104 (2010).
22. Anderson, D. M. *et al.* Using Amphiphilic Nanostructures To Enable Long-Range Ensemble Coalescence and Surface Rejuvenation in Dropwise Condensation. *ACS Nano* **6,** 3262–3268 (2012).
23. Ghosh, A., Beaini, S., Zhang, B. J., Ganguly, R. & Megaridis, C. M. Enhancing Dropwise Condensation through Bioinspired Wettability Patterning. *Langmuir* **30,** 13103–13115 (2014).
24. Paxson, A. T., Yagüe, J. L., Gleason, K. K. & Varanasi, K. K. Stable Dropwise Condensation for Enhancing Heat Transfer via the Initiated Chemical Vapor Deposition (iCVD) of Grafted Polymer Films. *Adv. Mater.* **26,** 418–423 (2014).
25. Bahadur, V. & Garimella, S. V. Electrowetting-Based Control of Static Droplet States on Rough Surfaces. *Langmuir* **23,** 4918–4924 (2007).
26. ’t Mannetje, D. *et al.* Trapping of drops by wetting defects. *Nat. Commun.* **5,** (2014).
27. Joseph, P. *et al.* Slippage of Water Past Superhydrophobic Carbon Nanotube Forests in Microchannels. *Phys. Rev. Lett.* **97,** 156104 (2006).
28. Mchale, Shirtcliffe, Evans & Newton. Terminal velocity and drag reduction measurements on superhydrophobic spheres. *Appl. Phys. Lett.* **94,** 064104 (2009).
29. Bhushan, B. Biomimetics inspired surfaces for drag reduction and oleophobicity/philicity. *Beilstein J. Nanotechnol.* **2,** 66–84 (2011).

30. Vakarelski, I. U., Patankar, N. A., Marston, J. O., Chan, D. Y. C. & Thoroddsen, S. T. Stabilization of Leidenfrost vapour layer by textured superhydrophobic surfaces. *Nature* **489,** 274–277 (2012).

31. Srinivasan, S. *et al.* Drag reduction for viscous laminar flow on spray-coated non-wetting surfaces. *Soft Matter* **9,** 5691–5702 (2013).

32. Solomon, B. R., Khalil, K. S. & Varanasi, K. K. Drag Reduction using Lubricant-Impregnated Surfaces in Viscous Laminar Flow. *Langmuir* **30,** 10970–10976 (2014).

33. Xu, W., Leeladhar, R., Kang, Y. T. & Choi, C.-H. Evaporation Kinetics of Sessile Water Droplets on Micropillared Superhydrophobic Surfaces. *Langmuir* **29,** 6032–6041 (2013).

34. Dicuangco, M., Dash, S., Weibel, J. A. & Garimella, S. V. Effect of superhydrophobic surface morphology on evaporative deposition patterns. *Appl. Phys. Lett.* **104,** 201604 (2014).

35. Sheffer, M., Groysman, A. & Mandler, D. Electrodeposition of sol–gel films on Al for corrosion protection. *Corros. Sci.* **45,** 2893–2904 (2003).

36. Xu, W., Liu, H., Lu, S., Xi, J. & Wang, Y. Fabrication of Superhydrophobic Surfaces with Hierarchical Structure through a Solution-Immersion Process on Copper and Galvanized Iron Substrates. *Langmuir* **24,** 10895–10900 (2008).

37. Milošev, I., Kosec, T. & Bele, M. The formation of hydrophobic and corrosion resistant surfaces on copper and bronze by treatment in myristic acid. *J. Appl. Electrochem.* **40,** 1317–1323 (2010).

38. Ishizaki, T., Masuda, Y. & Sakamoto, M. Corrosion Resistance and Durability of Superhydrophobic Surface Formed on Magnesium Alloy Coated with Nanostructured Cerium Oxide Film and Fluoroalkylsilane Molecules in Corrosive NaCl Aqueous Solution. *Langmuir* **27,** 4780–4788 (2011).
39. U.S. Department of Energy. *Monthly Energy Review*. (2015). at <http://www.eia.gov/totalenergy/data/monthly/pdf/sec7_5.pdf>
40. A Global Transition to Renewable Energy Will Take Many Decades. *Scientific American* at <http://www.scientificamerican.com/article/a-global-transition-to-renewable-energy-will-take-many-decades/>
41. International Energy Agency OECD Publications. *World Energy Outlook*. (2010).
42. E. Schmidt, W. Schurig, W. Sellschopp,. *Technische Mechanik und Thermodynamik*. **1, 53,** (1930).
43. Paxson, A. T. Condensation heat transfer on nanoengineered surfaces. (Massachusetts Institute of Technology, 2011). at <http://dspace.mit.edu/handle/1721.1/67630>
44. FAQ | National Hydropower Association. at <http://www.hydro.org/tech-and-policy/faq/#713>
45. Phillips, S., Darland, T., Sytsma M. *Potential Economic Impacts of Zebra Mussels on the Hydropower Facilities in the Columbia River Basin*. (Pacific States Marine Fisheries Commission, 2005).
46. G. H. Koch, M. Bringers, N. Thompson. *Corrosion Costs and Preventive Strategies in the United States*. (NACE, 2004).

47. NACE International. Historic Congressional Study: Corrosion Costs and Preventative Strategies in the United States, a Supplement to Materials Performance. in (2002).

48. Zhao, X. & Chen, X. D. *A Critical Review of Basic Crystallography to Salt Crystallization Fouling in Heat Exchangers. Heat Transfer Engineering*. (2013).

49. Kondrashov, V. & Rühe, J. Microcones and Nanograss: Toward Mechanically Robust Superhydrophobic Surfaces. *Langmuir* **30,** 4342–4350 (2014).

50. Liu, K. & Jiang, L. Metallic surfaces with special wettability. *Nanoscale* **3,** 825 (2011).

51. Azimi, G., Dhiman, R., Kwon, H.-M., Paxson, A. T. & Varanasi, K. K. Hydrophobicity of rare-earth oxide ceramics. *Nat. Mater.* **12,** 315–320 (2013).

52. Tian, Y. & Jiang, L. Wetting: Intrinsically robust hydrophobicity. *Nat. Mater.* **12,** 291–292 (2013).

53. Martínez, L. *et al.* Surface study of cerium oxide based coatings obtained by cathodic electrodeposition on zinc. *Appl. Surf. Sci.* **257,** 6202–6207 (2011).

54. Lawrence, N. J., Jiang, K. & Cheung, C. L. Formation of a porous cerium oxide membrane by anodization. *Chem. Commun.* **47,** 2703 (2011).

55. Azimi, G., Kwon, H.-M. & Varanasi, K. K. Superhydrophobic surfaces by laser ablation of rare-earth oxide ceramics. *MRS Commun.* **4,** 95–99 (2014).

56. Zenkin, S., Kos, Š. & Musil, J. Hydrophobicity of Thin Films of Compounds of Low-Electronegativity Metals. *J. Am. Ceram. Soc.* **97,** 2713–2717 (2014).

57. Good, R. J. Contact angle, wetting, and adhesion: a critical review. *J. Adhes. Sci. Technol.* **6,** 1269–1302 (1992).

58. Yuan, Y. & Lee, T. R. in *Surface Science Techniques* (eds. Bracco, G. & Holst, B.) 3–34 (Springer Berlin Heidelberg, 2013). at <http://link.springer.com/chapter/10.1007/978-3-642-34243-1_1>

59. Tyson, W. R. & Miller, W. A. Surface free energies of solid metals: Estimation from liquid surface tension measurements. *Surf. Sci.* **62,** 267–276 (1977).

60. Chibowski, E. Surface free energy of a solid from contact angle hysteresis. *Adv. Colloid Interface Sci.* **103,** 149–172 (2003).

61. Neumann, A. W. Contact angles and their temperature dependence: thermodynamic status, measurement, interpretation and application. *Adv. Colloid Interface Sci.* **4,** 105–191 (1974).

62. Applied Surface Thermodynamics, Second Edition. *CRC Press* at <https://www.crcpress.com/Applied-Surface-Thermodynamics-Second-Edition/Neumann-David-Zuo/9780849396878>

63. Schmidt, D. L., Brady, R. F., Lam, K., Schmidt, D. C. & Chaudhury, M. K. Contact Angle Hysteresis, Adhesion, and Marine Biofouling. *Langmuir* **20,** 2830–2836 (2004).

64. Avalon Rare Metals Inc. *RARE EARTHS 101: The Basics, Economics, Supply Chain and Applications*. at <http://avalonraremetals.com/_resources/pdf/REE101.pdf>

65. British Geological Survey. *Rare Earth Elements Profile*. at <https://www.bgs.ac.uk/downloads/start.cfm?id=1638>

66. Kung, H. H. *Transition Metal Oxides: Surface Chemistry and Catalysis*. (Elsevier, 1989).

67. Drzymala, J. Hydrophobicityand collectorless flotation of inorganic materials. *Adv. Colloid Interface Sci.* **50,** 143–185 (1994).

68. Hass, K. C., Schneider, W. F., Curioni, A. & Andreoni, W. The Chemistry of Water on Alumina Surfaces: Reaction Dynamics from First Principles. *Science* **282,** 265–268 (1998).

69. Giovambattista, N., Debenedetti, P. G. & Rossky, P. J. Effect of Surface Polarity on Water Contact Angle and Interfacial Hydration Structure. *J. Phys. Chem. B* **111,** 9581–9587 (2007).

70. Giovambattista, N., Debenedetti, P. G. & Rossky, P. J. Enhanced Surface Hydrophobicity by Coupling of Surface Polarity and Topography. *Proc. Natl. Acad. Sci.* **106,** 15181–15185 (2009).

71. Granick, S. & Bae, S. C. CHEMISTRY: A Curious Antipathy for Water. *Science* **322,** 1477–1478 (2008).

72. Azimi, G., Dhiman, R., Kwon, H.-M., Paxson, A. T. & Varanasi, K. K. Hydrophobicity of rare-earth oxide ceramics. *Nat. Mater.* **12,** 315–320 (2013).

73. Preston, D. J. *et al.* Effect of hydrocarbon adsorption on the wettability of rare earth oxide ceramics. *Appl. Phys. Lett.* **105,** 011601 (2014).

74. Tuteja, A. *et al.* Designing Superoleophobic Surfaces. *Science* **318,** 1618 –1622 (2007).

75. Chin, C. C. *et al.* On the off stoichiometry of cerium oxide thin films deposited by RF sputtering. *Phys. C Supercond.* **260,** 86–92 (1996).

76. Burroughs, P., Hamnett, A., Orchard, A. F. & Thornton, G. Satellite structure in the X-ray photoelectron spectra of some binary and mixed oxides of lanthanum and cerium. *J. Chem. Soc. Dalton Trans.* 1686 (1976). doi:10.1039/dt9760001686

77. Paparazzo, E. On the curve-fitting of XPS Ce(3d) spectra of cerium oxides. *Mater. Res. Bull.* **46,** 323–326 (2011).

78. Romeo, M., Bak, K., El Fallah, J., Le Normand, F. & Hilaire, L. XPS Study of the reduction of cerium dioxide. *Surf. Interface Anal.* **20,** 508–512 (1993).

79. Zhang, F., Wang, P., Koberstein, J., Khalid, S. & Chan, S.-W. Cerium oxidation state in ceria nanoparticles studied with X-ray photoelectron spectroscopy and absorption near edge spectroscopy. *Surf. Sci.* **563,** 74–82 (2004).

80. Bêche, E., Charvin, P., Perarnau, D., Abanades, S. & Flamant, G. Ce 3d XPS investigation of cerium oxides and mixed cerium oxide (CexTiyOz). *Surf. Interface Anal.* **40,** 264–267 (2008).

81. Preisler, E. J., Marsh, O. J., Beach, R. A. & McGill, T. C. Stability of cerium oxide on silicon studied by x-ray photoelectron spectroscopy. *J. Vac. Sci. Technol. B* **19,** 1611–1618 (2001).

82. Solovyov, V. F. *et al.* Highly efficient solid state catalysis by reconstructed (001) Ceria surface. *Sci. Rep.* **4,** (2014).

83. Reddy, B. M. *et al.* Structural Characterization and Catalytic Activity of Nanosized Ceria−Terbia Solid Solutions. *J. Phys. Chem. C* **112,** 16393–16399 (2008).

84. Fan, J., Wu, X., Yang, L. & Weng, D. The SMSI between supported platinum and CeO2–ZrO2–La2O3 mixed oxides in oxidative atmosphere. *Catal. Today* **126,** 303–312 (2007).

85. Khan, S., Azimi, G., Yildiz, B. & Varanasi, K. K. Role of surface oxygen-to-metal ratio on the wettability of rare-earth oxides. *Appl. Phys. Lett.* **106,** 061601 (2015).

86. Holgado, J. P., Munuera, G., Espinós, J. P. & González-Elipe, A. R. XPS study of oxidation processes of CeOx defective layers. *Appl. Surf. Sci.* **158,** 164–171 (2000).

87. Coronado, J. M., Javier Maira, A., Martínez-Arias, A., Conesa, J. C. & Soria, J. EPR study of the radicals formed upon UV irradiation of ceria-based photocatalysts. *J. Photochem. Photobiol. Chem.* **150,** 213–221 (2002).

88. Gionco, C., Giamello, E., Mino, L. & Paganini, M. C. The interaction of oxygen with the surface of CeO_2–TiO_2 mixed systems: an example of fully reversible surface-to-molecule electron transfer. *Phys Chem Chem Phys* **16,** 21438–21445 (2014).

89. Zhang, X. & Klabunde, K. J. Superoxide (O2-) on the surface of heat-treated ceria. Intermediates in the reversible oxygen to oxide transformation. *Inorg. Chem.* **31,** 1706–1709 (1992).

90. Joanny, J. F. & Gennes, P. G. de. A model for contact angle hysteresis. *J. Chem. Phys.* **81,** 552–562 (1984).

91. Lawrence, N. J., Jiang, K. & Cheung, C. L. Formation of a porous cerium oxide membrane by anodization. *Chem. Commun.* **47,** 2703 (2011).

92. Oh, I.-K. *et al.* Hydrophobicity of Rare Earth Oxides Grown by Atomic Layer Deposition. *Chem. Mater.* **27,** 148–156 (2015).

93. Cho, Y. J., Jang, H., Lee, K.-S. & Kim, D. R. Direct growth of cerium oxide nanorods on diverse substrates for superhydrophobicity and corrosion resistance. *Appl. Surf. Sci.* **340,** 96–101 (2015).

94. Matolín, V. *et al.* Growth of ultra-thin cerium oxide layers on Cu(1 1 1). *Appl. Surf. Sci.* **254,** 153–155 (2007).

95. Šutara, F. *et al.* Epitaxial growth of continuous CeO2(111) ultra-thin films on Cu(111). *Thin Solid Films* **516,** 6120–6124 (2008).

96. Mullins, D. R., Radulovic, P. V. & Overbury, S. H. Ordered cerium oxide thin films grown on Ru(0001) and Ni(111). *Surf. Sci.* **429,** 186–198 (1999).

97. Hardacre, C., Roe, G. M. & Lambert, R. M. Structure, composition and thermal properties of cerium oxide films on platinum {111}. *Surf. Sci.* **326,** 1–10 (1995).

98. Eck, S., Castellarin-Cudia, C., Surnev, S., Ramsey, M. G. & Netzer, F. P. Growth and thermal properties of ultrathin cerium oxide layers on Rh(1 1 1). *Surf. Sci.* **520,** 173–185 (2002).

99. Paxson, A. T. Advanced materials for enhanced condensation heat transfer. (Massachusetts Institute of Technology, 2014). at <http://dspace.mit.edu/handle/1721.1/92168>

100. Rose, J. W. Dropwise condensation theory and experiment: A review. *Proc. Inst. Mech. Eng. Part J. Power Energy* **216,** 115–128 (2002).

101. Sikarwar, B. S., Khandekar, S., Agrawal, S., Kumar, S. & Muralidhar, K. Dropwise Condensation Studies on Multiple Scales. *Heat Transf. Eng.* **33,** 301–341 (2012).

102. Rose, J. W. Some aspects of condensation heat transfer theory. *Int. Commun. Heat Mass Transf.* **15,** 449–473 (1988).